An agent-based model that simulates the spatio-temporal dynamics of sources and transfer mechanisms contributing faecal indicator organisms to streams. Part 2: Application to a small agricultural catchment

Aaron J. Neill[a,b], *Doerthe Tetzlaff*[c,d,a], *Norval J.C. Strachan*[e], *Rupert L. Hough*[b], *Lisa M. Avery*[b], *Marco P. Maneta*[f], *Chris Soulsby*[a,c]

[a] Northern Rivers Institute, University of Aberdeen, Aberdeen, AB24 3UF, Scotland, United Kingdom.

[b] The James Hutton Institute, Craigiebuckler, Aberdeen, AB15 8QH, Scotland, United Kingdom.

[c] IGB Leibniz Institute of Freshwater Ecology and Inland Fisheries, 12587 Berlin, Germany.

[d] Department of Geography, Humboldt University Berlin, 10099 Berlin, Germany.

[e] School of Biological Sciences, University of Aberdeen, Cruickshank Building, St Machar Drive, Aberdeen, AB24 3UU, Scotland, United Kingdom.

[f] Geosciences Department, University of Montana, Missoula, MT 59812-1296, USA.

Corresponding Author

Aaron J. Neill

aaron.neill@abdn.ac.uk

Northern Rivers Institute, University of Aberdeen, Aberdeen, AB24 3UF, Scotland, United Kingdom.

Highlights

- First test of agent-based model for simulating faecal indicator organisms (FIOs).
- Model shows skill in capturing transfer of FIOs from livestock to streams.
- Quantifies sources, transfer mechanisms and host animals for FIOs reaching streams.
- Potential to refine process conceptualisation (e.g. simulating FIOs from wildlife).
- Model likely has scope for eventual incorporation into decision-support frameworks.

Abstract

The new Model for the Agent-based simulation of Faecal Indicator Organisms (MAFIO) is applied to a small (0.42 km^2) Scottish agricultural catchment to simulate the dynamics of *E. coli* arising from sheep and cattle farming, in order to provide a proof-of-concept. The hydrological environment for MAFIO was simulated by the "best" ensemble run of the tracer-aided ecohydrological model EcH$_2$O-iso, obtained through multi-criteria calibration to stream discharge (MAE: 1.37 L s^{-1}) and spatially-distributed stable isotope data (MAE: 1.14-3.02‰) for the period April-December 2017. MAFIO was then applied for the period June-August for which twice-weekly *E. coli* loads were quantified at up to three sites along the stream. Performance in simulating these data suggested the model has skill in capturing the transfer of faecal indicator organisms (FIOs) from livestock to streams via the processes of direct deposition, transport in overland flow and seepage from areas of degraded soil. Furthermore, its agent-based structure allowed source areas, transfer mechanisms and host animals contributing FIOs to the stream to be quantified. Such information is likely to have substantial value in the context of designing and spatially-targeting mitigation measures against impaired microbial water quality. This study also revealed, however, that avenues exist for improving process conceptualisation in MAFIO (e.g. to include FIO contributions from wildlife) and highlighted the need to quantitatively assess how uncertainty in the spatial extent of surface flow paths in the simulated hydrological environment may affect FIO simulations. Despite the consequent status of MAFIO as a research-level model, its encouraging performance in this proof-of-concept study suggests the model has significant potential for eventual incorporation into decision support frameworks.

Key words:

Diffuse pollution; *E. coli*; EcH$_2$O-iso; Microbial water quality; Tracer-aided modelling; Water quality modelling

1. Introduction

A prerequisite to improving impaired microbial water quality in agricultural catchments is identification of the sources and transfer mechanisms which contribute faecal indicator organisms (FIOs) to streams at the sub-field scale where mitigation measures can be implemented (Oliver et al., 2007, 2016; also c.f. Greene et al., 2015; Vinten et al., 2017). In a companion paper (Neill et al., *in review*), limitations were identified in using existing process-based FIO models (e.g. SWAT [Sadeghi and Arnold, 2002] and INCA-Pathogens [Whitehead et al., 2016]) to understand sub-field-scale drivers of in-stream FIO dynamics that emerge at the catchment scale. Specifically, the coarse spatial discretisations often adopted by such models are inconsistent with the scales at which processes affecting FIO fate and transport operate and at which mitigation measures can be employed (Rode et al., 2010; Wellen et al., 2015). Furthermore, as most FIO models are aggregative (i.e. they simulate stores and fluxes of FIOs integrated over spatial units such as grid cells), the ability to account for heterogenity amongst FIOs of different types and to trace pathways taken by individual FIOs to streams is limited (c.f. O'Sullivan et al., 2012; Reaney, 2008). Finally, most FIO models rely on skill in simulating stream discharge to indicate whether catchment hydrological functioning is being adequately captured (Cho et al., 2016). However, such data do not contain information on the velocities of water through a catchment that reflect flow path dynamics and hydrological connectivity, factors to which FIO transport is sensitive (Birkel and Soulsby, 2015; Wellen et al., 2015).

Drawing on the potential offered by agent-based models for simulating individuals with heterogenous attributes that can be tracked over a simulation, Neill et al. (*in review*) reported the development of a new Model for the Agent-based simulation of Faecal Indicator Organisms (MAFIO) as an alternative approach to FIO modelling. The purpose of the model is to elucidate the sources and transfer mechanisms contributing FIOs to streams at the sub-field scale in small (<10 km^2) agricultural catchments through simulating and tracking the fate and transport of agents representing FIOs (FIO-agents) in a process-based, spatially-distributed manner. MAFIO consists of six sub-models that allow simulation of the following processes: 1) FIO loading from different livestock, including direct deposition in streams; 2) FIO die-off as a function of temperature and, for above-ground FIOs, solar radiation; 3) Precipitation-induced detachment of FIOs from faeces; 4) Surface routing of FIOs accounting for infiltration, exfiltration and lateral transport in overland flow; 5) Seepage of FIOs to streams from areas of degraded soil; 6) Channel routing with settling modelled by a distance-decay function for sediment-associated FIOs. A further key feature of MAFIO is that the hydrological environment used to simulate hydrological transfer mechanisms is provided by an external model; thus, there is scope for using hydrological models which can be robustly evaluated with respect to their

consistency with internal catchment states and process representation. Full details of the model, its operation and parameterisation can be found in the companion paper (Neill et al., *in review*).

Here, MAFIO is applied to simulate the dynamics of *E. coli* in a small agricultural catchment in Scotland arising from sheep and cattle farming, in order to provide a proof-of-concept. The following specific questions are addressed:

1. To what extent can MAFIO resolve the main processes driving observed dynamics of FIOs?
2. What potential does MAFIO have for providing processed-based insights into microbial water quality that are relevant for management?

Given the potential of tracer-aided ecohydrological models in providing robust simulations of catchment hydrological functioning (see Neill et al., *in review*), the model EcH$_2$O-iso (Kuppel et al., 2018a) is used to generate the hydrological environment for MAFIO following multi-criteria calibration to discharge and spatially-distributed isotope data.

2. Study site

The study site was the Tulloch Burn catchment (0.42 km^2; Figure 1a), a sub-catchment of the Tarland Burn (71 km^2) which is a tributary of the River Dee, NE Scotland. The Dee is a regional water resource, supplying >300,000 people with drinking water, and is designated a Special Area of Conservation due to the freshwater ecosystem it supports. Higher intensities of agriculture in lowland tributaries of the Dee have been linked to impaired water quality (Langan et al., 1997). As the most upstream tributary draining significant areas of agriculture, the Tarland Burn catchment became a research site for assessing diffuse- and point-sources of pollution and evaluating best management practices for mitigation (Bergfur et al., 2012). The selection of the Tulloch Burn catchment for this study was based on work that identified it as a "hot spot" for faecal contamination from 11 years of *E. coli* data (Neill et al., 2018).

Longer-term data (2000-2010) from Aboyne meteorological station ~10 km from the Tulloch shows mean annual precipitation and potential evapotranspiration for the area to be 828 mm and 521 mm, respectively (Dunn et al. 2013). Catchment elevation ranges from 216 m to 453 m. Brown earths (41%)

and humus-iron podzols (34%) are the predominant soil-types (Figure 1b; Soil Survey of Scotland Staff, 2014). These are freely-draining soils; consequently, artificial field drainage is not necessary in the catchment. There are also limited areas of non-calcareous gleys and alluvial soils, with higher elevations dominated by peaty-gleyed podzols (Figure 1b; Soil Survey of Scotland Staff, 2014). Approximately 60% of the catchment is agricultural (Figure 1c). During the study, surveys showed that five fields were used for pastoral (sheep and cattle) farming (Lower/Mid Pasture [L/R] and Top Pasture) and two for arable (Lower/Upper Arable). Apart from Mid-Pasture (R), field boundaries extend beyond the Tulloch Burn catchment. Of the remaining catchment, 24% is mixed-conifer forest and 16% is heather moorland (Figure 1c).

To prevent livestock access, parts of the stream are fenced-off from fields and surrounded by small riparian areas (Figure 1d). However, stretches of the stream running through Mid Pastures (R) and (L) are directly accessible to livestock, with animals able to move between Mid Pastures (R) and (L) at a discrete stream crossing-point depending on whether a gate is open (Figure 1c and e). Other discrete crossing-points can also connect Lower Pastures (R) and (L), and Lower Pasture (L) and Mid Pasture (R), again depending on gates (Figure 1c). Observation during the study found a high degree of soil compaction around all three crossing points (DS1-3 in Figure 1c) due to the concentration of livestock moving through these areas. This resulted in the soils being in a state of semi-permanent saturation (Figure 1f); therefore, these areas of degraded soil can continually seep water to the stream and may be a potential source of chronic faecal contamination (e.g. Bilotta et al., 2007).

3. Data and methods

3.1 Hydrometric and isotope data

Hydrometric monitoring at the Tulloch Burn started in October 2016. The main study period was between 27/04/17 and 31/12/17. Daily average discharge at the catchment outlet and sites T6 and T8 was derived by area-scaling discharge measurements made at the outlet of the 3.9 km^2 Blackmill Burn catchment within which the Tulloch is nested. Specifically, near-concurrent discharge (Q) measurements made under identical hydroclimatic conditions at five sites within the Blackmill Burn (including the outlet of the Tulloch) with catchment areas (A) of 0.2-3.9 km^2 revealed a strong relationship between discharge and area ($Q = 1.85e\text{-}8 \times A^{0.97}$; Adj. R^2: 0.99). Consequently, discharges for sites within Tulloch Burn could be derived as:

$$Q_{TulX} = Q_{BM} \cdot \left(\frac{A_{TulX}}{A_{BM}}\right)^{0.97} \quad Eq.1$$

where Q_{TulX} and A_{TulX} are discharge and catchment area for Site *X* in the Tulloch Burn, respectively, and Q_{BM} and A_{BM} are discharge and catchment area of the Blackmill Burn, respectively. This was necessary as the narrow, poorly-defined channel of the Tulloch prevented a reliable stage-discharge rating curve. The Blackmill and Tulloch Burns have comparable soils and land use causing them to exhibit similar hydrological responses. Meteorological data (precipitation, temperature, relative humidity and windspeed) were collected at 15-mintue intervals using an automatic weather station within the catchment (Figure 1a). Short- and long-wave radiation were obtained from ERA-Interim climate reanalysis (Dee et al., 2011). These data were amalgamated into daily timeseries.

Isotope samples were analysed for δ^2H and $\delta^{18}O$ using a Los Gatos laser isotope analyser (precision: ± 0.4‰ for δ^2H and 0.1‰ for $\delta^{18}O$). Given higher relative precision, δ^2H was used here. Daily streamwater samples at the catchment outlet were collected for isotope analysis using an ISCO-3700 autosampler from 27/04/17 (Figure 1a). A layer of paraffin was added to bottles to prevent evaporation. Synoptic grab-sampling for isotopes occurred on a twice-monthly basis at sites T2-8 (Figure 1a). During the microbial observation period (Section 3.2), samples were taken twice-weekly at T6 and T8 to be coincident with samples taken for *E. coli* analysis. Daily bulk samples of precipitation were also collected using an ISCO-3700 autosampler.

3.2 Microbial and livestock count data

Within the study, a more intense field campaign was carried out between 08/06/17 and 31/08/17 (the "microbial observation period" – MOP) to collect higher-temporal-resolution data for stream *E. coli* concentrations and livestock counts. This corresponded to when most livestock are in the fields and potential for faecal contamination is elevated (Kay et al., 2008). Twice-weekly sampling for *E. coli* occurred during this period at the outlet, and from 06/07/17 at T6 and T8 to characterise spatial variability in concentrations arising from differing catchment characteristics (Figure 1a). Samples for *E. coli* were collected (working upstream to T8) in glass bottles sterilised by autoclaving at 123 °C for 20 minutes. Care was taken not to disturb the channel bed to prevent contamination from *E. coli* stored in the sediment. Samples were placed in cool boxes until processing began within 6 hours of collection. Concentrations of *E. coli* were determined using the Colilert-18 most-probable-number (MPN) method (IDEXX Laboratories, Westbrook, Maine, USA). Samples were well-shaken to ensure uniform distribution of *E. coli* prior to 100 ml being decanted to provide concentrations in MPN 100 ml^{-1}. When

high concentrations of *E. coli* were likely, dilutions were made using sterile Ringers' solution. The limit of detection for undiluted samples was 1 MPN 100 ml^{-1}. *E. coli* loads (MPN d^{-1}) were derived by multiplying observed concentrations of *E. coli* at the outlet, T6 and T8 by average daily discharge for each respective site.

Number and type of livestock in each agricultural land parcel of the catchment (Figure 1c) was recorded each sampling day. Where a land parcel represented a field with boundaries that extended beyond the Tulloch Burn catchment, the total number of livestock in the whole field was scaled by the fraction of the field falling within the land parcel. This assumed livestock would be uniformly distributed within a given field (c.f. Dorner et al., 2006; Haydon and Deletic, 2006). If livestock could move between land parcels, then the total number of livestock in all connected parcels was counted and scaled to each individually based on the fraction of the total connected area they represented. In addition, whether gates prevented livestock access to the stream at crossing points DS1-3 (Figure 1c) was also recorded. The remainder of the stream was either fenced off and inaccessible to livestock, or, for stream sections in Mid Pastures (L) and (R), permanently open to livestock (Figure 1c and e). Daily timeseries of stream access and livestock counts were generated from the twice-weekly observations by assuming any changes occurring between successive observation days did so at the mid-point between them.

3.3 Setup of EcH_2O-iso for the Tulloch Burn

In EcH_2O-iso, the spatial grid for simulations is defined by a digital elevation model (Kuppel et al., 2018a). A 5×5 m resolution LandMap digital terrain model (DTM) was resampled to 30×30 m resolution for delineating the Tulloch Burn catchment and deriving local slopes and drainage directions. The relatively coarse spatial resolution was necessary to keep model runtimes manageable given the long spin-up period needed for simulated water ages to stabilise. Simulation of 22 years with a daily timestep was necessary, with the period 27/04/17 to 31/12/17 for the last year retained for further analysis. The 22-year spinup was achieved by looping meteorological and isotopic inputs for 2016-2017 eleven times (c.f. Hrachowitz et al., 2010). Meteorological data before establishment of a catchment weather station (October 2016) were derived from the adjacent Aboyne and Bruntland Burn stations using statistical relationships from periods of overlapping data, whilst radiation for all of 2016 was available from the ERA-Interim climate reanalysis. For altitudinal effects on precipitation and temperature, a 5.5% increase in precipitation (Ala-aho et al., 2017) and decrease of 0.6 °C (Goody and Yung, 1995) with every 100 metre elevation gain was implemented.

Parameterisation of soil hydrological properties in EcH_2O-iso was based on the five mapped soil types in the catchment (Soil Survey of Scotland Staff, 2014; Figure 1b). Soil properties were assumed to be uniform within each type. To facilitate parameterisation of vegetation, land parcels of the Tulloch Burn in Figure 1c were divided into three categories: agriculture, forest and heather moorland. Based on local knowledge, agricultural areas were assumed to comprise 95% grass and 5% bare soil, forested land was assumed to comprise 68% conifers, 30% grasses and 2% bare soil, and heather moorland was assumed to comprise 95% heather and 5% bare soil. To identify parameters for calibration, an initial sensitivity analysis was undertaken following the method of Morris (1991) and Sohier et al. (2014) using eight trajectories and a radial step for evaluating the parameter space. This identified 11 soil-related, 13 vegetation-related and two channel-related parameters as sensitive (Table S1), resulting in the need to calibrate 96 individual parameter values ([11×5]+[13×3]+2=96). Values of fixed parameters are given in Table S2.

3.4 Multi-criteria calibration of EcH_2O-iso

Calibration of the 96 parameter values followed a multi-criteria approach incorporating stream discharge (outlet) and δ^2H (outlet + sites T2-8) as calibration targets. Latin Hypercube Sampling was used to generate 100,000 parameter sets for EcH_2O-iso, based on the sampling ranges given in Table S1. For each model run, mean absolute errors (MAEs; Willmott and Matsuura, 2005) were calculated to quantify the skill of the run in simulating the dynamics of each calibration target for the period 27/04/17 to 31/12/17. For discharge, use of MAE avoided overemphasis on high-flows typical of alternatives such as the Nash-Sutcliffe efficiency statistic (Krause et al., 2005; Legates and McCabe, 1999), whilst for isotopes the limited variability in observations and daily timestep of the model necessitated use of a measure of average error (c.f. Gupta et al., 2009; Schaefeli and Gupta, 2007). A single performance metric for each model run was then derived by combining MAEs for individual calibration targets via a weighted-addition (e.g. Beven, 2012). This allowed the number of observations for each calibration target to determine the influence of its associated MAE on defining overall performance of the run and enabled identification of a "best" run for use in providing the hydrological environment for MAFIO (Section 3.5.2).

As MAE is dimensional with an optimal value of 0, it was necessary to convert the MAEs associated with each calibration target into dimensionless metrics that monotonically increase with model performance, prior to implementing the weighted addition. The latter need was met by calculating the metric (1-MAE), which increases with model performance to an optimum of 1 (in both instances 1 is in units of the calibration target). To remove dimensionality and obtain a metric (MAE^*) for use in the weighted addition, the following equation was applied:

$$MAE^*_{i,j} = \frac{\left(1 - MAE_{i,j}\right) - \min(1 - MAE)_j}{\max(1 - MAE)_j - \min(1 - MAE)_j} \qquad Eq.2$$

where $MAE_{i,j}$ is the MAE associated with calibration target j for model run i and $(1\text{-}MAE)_j$ is the complete set of (1-MAE) associated with calibration target j from all 100,000 model runs. For a given run, a final goodness of fit in the range [0,1] was obtained through the weighted addition:

$$GOF_i = \sum_{j=1}^{n} W_j . MAE^*_{i,j} \qquad Eq.3$$

where GOF_i is the goodness of fit value of run i and W_j is the weighting given to the performance metric MAE^* associated with calibration target j. The weighting of a performance metric associated with a given calibration target was the fraction of observations for all calibration targets that it contained. Numbers of observations and consequent weightings for each target used in the calibration are detailed in Table 1. Following calibration, an ensemble of the 100 model runs with the highest *GOF* values (behavioural runs) were retained to examine model performance and uncertainty.

3.5 Setup of MAFIO for the Tulloch Burn

As a first test of the model, MAFIO was used to simulate the behaviour and transport of *E. coli* in the Tulloch Burn during the MOP. This section describes the setup of the catchment and hydrological environments of the model (see Section 3.2 of Neill et al., *in review*) and its parameterisation for *E. coli*.

3.5.1 Catchment environment

Table 3 of Neill et al. (*in review*) outlines the inputs necessary to characterise the catchment environment. Catchment extent and local drainage directions were defined from the 30×30 m DTM (identical to EcH_2O-iso). The spatial distribution of land parcels and of cells containing degraded soil / the channel were defined as shown in Figure 1c. To facilitate representation of sub-grid heterogeneity in the latter, channel widths were derived from linear interpolation between field measurements of bankfull width. In addition, land parcels either adjacent to the stream (stream-associated land parcels)

289 or from which livestock could contribute to soil degradation were defined as those falling within the
290 30×30 m footprint of a given cell as determined from field observations and aerial imagery (Table S3).
291 The cell(s) immediately upslope of those containing degraded soil / the channel were defined from local
292 drainage directions (Figure S1). Timeseries of livestock counts and access to the stream were as
293 described in Section 3.2.

294

295 *3.5.2 Hydrological environment*

296 The hydrological environment of MAFIO was simulated by the "best" overall ensemble run of EcH_2O-
297 iso. To qualitatively assess the potential for uncertainty in the outputs of EcH_2O-iso to impact MAFIO
298 simulations, spatial patterns of surface and groundwater flow paths and soil saturation deficit simulated
299 over the MOP by the "best" run and by the 100 behavioural runs were compared. This indicative
300 approach was taken as a full quantitative uncertainty analysis would require using the 100 behavioural
301 EcH_2O-iso runs to generate the hydrological environment for an ensemble of MAFIO runs, the latter
302 necessary to account for the effect of stochasticity (see Section 3.6). Such an uncertainty analysis was
303 beyond the scope of this initial proof-of-concept test of MAFIO; however, this will be a focus of future
304 work. To aid in assessing process representation in MAFIO, the simulated hydrological environment
305 was characterised by generating spatial summaries of discharge, δ^2H and water ages in the stream, and
306 of overland flow, soil saturation deficit and groundwater fluxes within the catchment, for the whole
307 MOP and for exemplar "dry" (10/08/17) and "wet" (15/08/17) days. Here, streamwater ages denote
308 how long water contributing to discharge spent travelling through the catchment since entering it as
309 precipitation (Sprenger et al., 2019).

310

311 *3.5.3 Parameterisation of MAFIO sub-models*

312 Parameter values for the MAFIO sub-models are presented in Table 4 of Neill et al. (*in review*). Sheep
313 and cattle were the only livestock reared in the catchment. Most parameter values were taken from the
314 extensive literature on *E. coli* as an FIO. Exceptions were the parameters *faecesConc* (concentration of
315 FIOs per gram of faeces) and *agentsRepresent* (number of FIOs shed in reality for which an FIO-agent
316 is introduced into the simulation). For the former, geometric mean concentrations of *E. coli* in sheep
317 and cattle faeces were determined from faecal samples collected in the catchment during 2017 and 2018
318 (Avery et al., *unpublished data*). Meanwhile, the minimum value of *faecesConc* (4.18×10^5) was used
319 for *agentsRepresent*. This was the minimum permissible value given available computational resources;
320 however, similarities between simulations obtained using this value and a value of 1×10^8 *E. coli* (*Data*
321 *not shown*) suggested that significant changes to model outputs would be unlikely if a smaller value
322 were to be used. This provided confidence that a sufficient quantum of *E. coli* was simulated by MAFIO.

Despite potential uncertainty in the values of model parameters (Oliver et al., 2016), calibration was not undertaken in this initial application. This was primarily because use of stochasticity to model processes conceptualised in ABMs hinders the use of "fit-to-data" metrics (i.e. those quantifying model skill in reproducing dynamics of observed data) often used in automated calibration (Polhill and Salt, 2017). This is further described in Section 3.6. A benefit to using the model uncalibrated is that it offers insight into the process consistency of the model if physically-meaningful parameter values are used (c.f. Kuppel et al., 2018a), as compensatory parameter effects on model structural deficiencies from calibration are avoided (c.f. Beven, 2019).

3.6 Application of MAFIO

MAFIO was applied for the MOP on a 30×30 m spatial grid using a daily time step, consistent with the spatio-temporal resolution of data characterising the catchment and hydrological environments. For initialisation, values for the fraction of damaged soil (*dFrac*) at DS1, DS2 and DS3 were set to 0.72, 0.53 and 0.7155, respectively, based on application of Eq. 3 of Neill et al. (*in review*) with livestock counts made in the catchment since 01/01/17. As these counts also showed all pasture land parcels to have been grazed to some extent since the start of 2017, all were set to have FIO-agents already in the soil at initialisation as a significant soil reservoir of *E. coli* may persist for several months even after cessation of grazing (Muirhead, 2009). Initial numbers of FIO-agents were based on estimates of the total number of *E. coli* in the upper soil of each land parcel (between 4.1×10^{9} - 9.3×10^{10} *E. coli*). These were approximated from concentrations of *E. coli* (in MPN g^{-1}) measured in the top 5 cm of soil at five locations within the Lower and Mid Pasture fields (Avery et al., *unpublished data*) and estimates of the weight of soil in each land parcel over the same depth.

An ensemble of 30 model runs using the same parameterisation and input was made for the MOP to characterise stochastic variability in MAFIO outputs (Abdou et al., 2012). Combined with the fact that natural variability intrinsic to complex systems can cause observed data to be conditional on a particular trajectory having been taken by the system, of which many may have been possible (Refsgaard et al., 2007; Windrum et al., 2007), this stochastic variability characteristic of ABM outputs can complicate assessments of model performance (Brown et al., 2005). In particular, traditional "fit-to-data" metrics become inappropriate as exclusive means of evaluating ABM performance as a model that adequately represents the processes giving rise to observations could be unfairly penalised if, due to stochastic treatment of system processes, it simulates a range of plausible scenarios which may or may not include what was observed (Polhill and Salt, 2017). Whilst a "benchmark" alternative is yet to emerge, other ABM work has highlighted the value of combining quantitative performance evaluation with qualitative "checks" that focus on understanding how simulated characteristics at larger scales emerge

from the processes influencing the behaviour of individual agents and assessing the plausibility of such processes similarly effecting the phenomena under investigation in reality (Moss and Edmonds, 2005; Polhill et al., 2010; Polhill and Salt, 2017).

Consequently, the following approach to performance assessment was adopted. For each ensemble run, observed and simulated *E. coli* loads were compared quantitatively at the outlet, T6 and T8. Since MAFIO simulates fluxes of FIO-agents, simulated loads were approximated by multiplying FIO-agent fluxes by the value of *agentsRepresent*. As this parameter dictates the precision to which observed loads can be simulated (c.f. Parry and Bithell, 2012), the skill of MAFIO in capturing periods of relatively more or less impaired microbial water quality was also assessed (c.f. Oliver et al., 2010; Porter et al., 2017). This was achieved by calculating Z-scores showing the number of standard deviations an observed *E. coli* load or simulated flux of FIO-agents was away from the mean of its associated timeseries. As observations were not available for all dates, Z-scores for simulated FIO-agent fluxes were based only on simulations that overlapped with observations. Spearman's rank correlation coefficients were also used to assess how well MAFIO captured the relative order of observed *E. coli* loads at each site (c.f. Porter et al., 2017). For a qualitative "check" on the model, the plausibility of simulated outputs given the potential processes influencing *E. coli* dynamics in the Tulloch Burn was the subject of a literature-based discussion (Section 5.1) that also considered the performance of EcH_2O-iso in simulating the hydrological environment. Whilst such qualitative evaluation is less robust than alternative methods based on consultation of independent experts (e.g. Moss and Edmonds, 2005; Polhill et al., 2010), the latter was beyond the scope of this initial MAFIO application.

As a basis for assessing the potential of MAFIO in providing insights relevant to management, the overall flux of FIO-agents leaving the catchment in the stream ("exported FIO-agents") was observed and further disaggregated into contributions from different livestock types and transfer mechanisms. The latter were derived from the attributes *Domain type* and *Livestock type* (see Table 2 of Neill et al., *in review*) of exported FIO-agents. By observing the *Location memory* attribute, areas where exported FIO-agents entered the stream via direct deposition and pathways taken by exported FIO-agents reaching the stream in overland flow or seepage were also identified. For each timestep, pathways were derived by quantifying the total number of exported FIO-agents that had passed through each grid cell in overland flow or seepage at any point whilst being transported from their original spawning location to the stream (i.e. pathways reflect the transport of exported FIO-agents over their entire existence, not just during the timestep in which they were exported). Meanwhile, spatial patterns of direct deposition were characterised by quantifying the total number of exported FIO-agents entering the stream via direct deposition for each cell containing a channel. For each of the 30 ensemble runs of MAFIO, timestep

totals were extracted for the example dry and wet days and further summed over the whole MOP. Median totals across the ensemble runs for each cell were then used to generate "average" maps of direct deposition and pathways taken to the stream by exported FIO-agents for each period of interest, whilst maps using ranges in totals were generated to evaluate the effect of stochastic variability in ensemble simulations.

4. Results

4.1 Hydrometric and isotope observations

Hydroclimatic conditions in 2017 were typical for the region (Hannaford et al., 2018). The study period started out relatively dry, with only 23 mm of precipitation falling by the end of May (Figure 2a). Consequently, summer baseflows were established by mid-June (Figure 2b), despite the largest precipitation event of the study (37.2 mm d^{-1}) occurring at the beginning of that month, two days before the MOP commenced. For the remaining summer, precipitation fell in low-intensity events that generated small discharge responses (Figure 2a-b and 3a). Sustained periods of precipitation in mid-September re-wetted the catchment leading to a rise in baseflows and the largest discharge responses (up to 31 L s^{-1}) being observed in November (Figure 2a-b).

The δ^2H composition of precipitation ranged between -153.1‰ and -14.9‰ (Figure 2a). By contrast, the δ^2H composition of stream water at the outlet was substantially damped (range -64.2‰ to -55.0‰), though deviations in the direction of the precipitation signal were observed during events (Figure 2b). At T2-8, δ^2H was similarly damped, ranging between -61.0‰ and -54.8‰ across all sites (Figure 2c). These sites behaved similarly to the outlet in terms of variability; however, the upper T7 and T8 sites had slightly more enriched δ^2H values, with values then becoming more depleted towards the outlet (Figure 2c). Daily average air temperatures peaked at ~18 °C in May and June and fluctuated ~12 °C until September when temperatures fell towards a minimum of -3 °C in December (Figure 2d). Solar radiation followed a similar trajectory (Figure 2d).

4.2 Microbial observation period (MOP)

Microbial observations began as the hydrograph experienced a small secondary peak in response to precipitation that occurred following the 37.2 mm d^{-1} precipitation event (Figures 2a-b and 3a). Peak daily average temperature and solar radiation for the overall study period fell within the MOP, with the former averaging 12.7 °C and the latter 176 W m^{-2} (Figure 3b).

Temporal dynamics of *E. coli* concentrations and loads at individual sites were similar (Figure 3c-d). At the outlet, concentrations ranged from 2.3×10^{1} to 2.0×10^{3} MPN 100 ml^{-1} (Figure 3c), whilst loads varied between 4.9×10^{7} and 4.1×10^{9} MPN d^{-1} (Figure 3d). Both were highest towards the end of the MOP and lowest during early July. The latter coincided with no livestock present in fields closest to the catchment outlet (Figures 1c and 3f), suggesting that this period may have been characterised by background concentrations of *E. coli*. At T6, concentrations and loads varied between 4.4×10^{1} and 9.1×10^{3} MPN 100 ml^{-1} and 5.0×10^{7} and 8.7×10^{9} MPN d^{-1}, respectively (Figure 3c-d). Thus, whilst T6 and the outlet generally experienced similar concentrations and loads of *E. coli*, these could be higher at the former site. T8 was generally the least-contaminated site as concentrations of *E. coli* were <10 MPN 100 ml^{-1} on over half the sampling days (Figure 3c). However, concentrations could increase to 10^{2} MPN 100 ml^{-1}, most frequently towards the end of the MOP. Loads varied between 5.8×10^{5} and 3.9×10^{8} MPN d^{-1} (Figure 3d) and were, consequently, often much smaller than loads observed at the outlet and T6 (exceptions are the last three sample dates of the MOP where loads at T8 were greater than at T6). A clear response of *E. coli* concentrations and loads to discharge was elusive; however, a link to livestock counts was more apparent at the outlet and T6.

Timeseries showing stream accessibility to livestock at the three discrete crossing points are shown in Figure 3e. Sheep were the main livestock in the catchment and were in Lower Pasture (L), Mid Pasture (R), Top Pasture or, for a short time late in the MOP, Lower Pasture (R) (Figure 3f). Cattle were briefly present in Mid Pasture (R) from late June to early July (Figure 3f).

4.3 Multi-criteria calibration of EcH$_2$O-iso

The results of calibrating EcH$_2$O-iso to discharge and spatially-distributed isotope data are summarised in Table 2 and Figure 4; calibrated parameter ranges are given in Table S1. Discharge was generally well-simulated (Table 2), with behavioural model runs successfully capturing the summer baseflows and small events that characterised the MOP alongside the re-wetting of the catchment in September and timing of the largest discharges in November (Figure 4b). The magnitudes of the latter were, however, under-estimated, as were discharges at the start of the simulation period (Figure 4b). For isotopes, the model could reproduce the markedly-damped composition of streamwater at the outlet (Table 2; Figure 4c). Isotopic variability in response to precipitation was also generally well-captured, though more extreme excursions could be simulated. Skill in simulating isotope dynamics at the synoptic sampling sites was more variable (Table 2; Figure 4d-j), likely reflecting their lower weighting in the multi-criteria calibration (Table 1) and the sparser temporal resolution of observations.

Performance was best for sites closer to the outlet, whilst simulations for sites further upstream showed greater uncertainty with some ensemble runs exhibiting poorer performance. However, performance was still maintained in the "best" overall run, with MAEs not exceeding ~3‰ at the upstream sites (Table 2). Overall, it was encouraging that EcH$_2$O-iso generally reproduced the damped isotope signals observed at the synoptic sampling sites.

4.4 Characterisation of the hydrological environment

Median discharges over the MOP (Figure 5a) simulated by the "best" run of EcH$_2$O-iso decreased in age with distance downstream (Figure 5e) but did not exhibit a clear spatial pattern in δ^2H (Figure 5c). Median streamwater ages were relatively old (averaging ~1.5 years), reflecting the dominant simulation of groundwater fluxes over surface water fluxes. Overland flow was only simulated for very restricted areas, mainly limited to stream-proximal cells in the lower part of the catchment (Figure 5b). Over the MOP, cells for which overland flow was simulated generated total fluxes <1000 mm. By contrast, simulated groundwater fluxes over the MOP could be up to 4700 mm for individual cells and occurred across much of the catchment (Figure 5f). The limited extent of simulated overland flow arose from much of the soil in the catchment being in saturation deficit (Figure 5d). Highest deficits were generally simulated in the upper catchment in areas of forest and heather (Figure 1c) underlain by podzolic soils (Figure 1b); here, overland and groundwater fluxes were consequently minimal (Figure 5b and f).

Stream discharges simulated for the example wet day were higher than for the dry day (Figure 6a) and consisted of younger water (median age of streamwater 399 days vs. 522 days; Figure 6e). The isotopic composition of the stream was also generally more enriched in wet conditions (Figure 6c). This, together with the lower streamwater ages, indicates increased contributions of younger overland flow and soil water to streamflow during summer wet conditions compared with the dominance of older groundwater during drier periods. However, even when wet, overland flow remained spatially limited, with just a few cells adjacent to the stream and a small number of distal, unconnected cells simulating fluxes of up to 35.7 mm d^{-1} (Figure 6b). In dry conditions, overland flow was generated from more restricted areas that maintained saturation by virtue of their position in flatter parts of the riparian area (Figure 6b). Overland flow was limited due to most soil being in saturation deficit in both dry and wet conditions (Figure 6d). In contrast, groundwater fluxes were active across similar spatial areas on the wet and dry days, with fluxes of up to 57.8 mm d^{-1} and 35.7 mm d^{-1} simulated for each day, respectively (Figure 6f).

Assessment of the spatial outputs from the 100 behavioural runs of EcH$_2$O-iso revealed that generation of overland flow from areas proximal to the stream and the dominance of groundwater simulated by the

493 "best" run was also simulated with reasonable certainty (i.e. in >50% of runs) by the ensemble (Figure
494 7a-c). In addition, relative spatial patterns of moisture deficits were comparable (Figure 7d). However,
495 it was possible for some behavioural runs to simulate larger areas of overland flow generation, leading
496 to uncertainty in the exact spatial extent of surface flow paths (Figure 7c). The implications of this will
497 be discussed with respect to assessing the adequacy of process conceptualisation in MAFIO.

498

499 *4.5 Performance of MAFIO*

500 Simulated *E. coli* loads at the outlet captured the main dynamics of observations quite well; in particular,
501 the observed decrease in loads in early July and subsequent increase, relatively constant loads in early-
502 to mid-August, and brief dip in loads towards the end of the MOP were all simulated (Figure 8a).
503 However, there was a general tendency for loads to be over-predicted, with the main exceptions being
504 at the end of the MOP and when observed loads decreased in July (Figure 8a). Z-scores at the outlet
505 show that the model was more successful in capturing when loads were above- and below-average, with
506 the sign of the Z-scores simulated correctly in the majority of cases (Figure 8b). Exceptions were at the
507 end of the simulation (reflecting over-prediction of observed loads earlier on despite absolute loads at
508 the end of the MOP being successfully captured) and on 03/07/17. Spearman's rank correlations ranged
509 between 0.21 and 0.30 with an average of 0.26 across the 30 ensemble runs. Stochastic variability in
510 outlet simulations was minimal (Figure 8a-b).

511

512 At T6, all ensemble runs simulated loads of zero and Z-scores below 0 whenever livestock were absent
513 from Mid Pastures (R) or (L) (Figures 3f and 8c-d). Non-zero loads were only simulated when Mid
514 Pasture (R) had livestock present (Figures 3f and 8c); however, simulated loads and Z-scores exhibited
515 a high degree of stochastic variability (Figure 8c-d). Consequently, Spearman's rank correlations varied
516 between runs, ranging from -0.12 to 0.32. When livestock were present in Mid Pasture (R), observations
517 generally fell within simulation bands; however, loads were under-estimated when livestock were
518 absent (Figure 3f and 8c). For relative performance, observed Z-scores were often within the range
519 simulated (Figure 8d). When non-zero loads were simulated, the large range in simulated Z-scores
520 meant that MAFIO was not consistent between ensemble runs in terms of simulating loads above- or
521 below-average. At the end of the period, observed and simulated Z-scores were similar, suggesting that
522 MAFIO successfully captured this as a time of relatively less-impaired microbial water quality.

523

524 Ensemble runs always simulated zero loads at T8 (Figure 8e). Consequently, neither Z-scores for
525 MAFIO simulations nor Spearman's rank correlations could be calculated. Qualitatively, the simulated
526 behaviour was largely consistent with the low concentrations and loads of *E. coli* at T8 (Figure 3c-d),

and negative observed Z-scores (Figure 8f). Quantitatively, however, the simulation of zero loads was not consistent with observations.

4.6 Sources and mechanisms contributing E. coli to streams

To help interpret timeseries relating to exported FIO-agents, simulated effective precipitation, discharge at the outlet and storage of FIO-agents are shown in Figures 9a-b. The simulated flux of exported FIO-agents (Figure 9c) strongly reflected storage dynamics of FIO-agents (Figure 9b) and livestock counts (Figure 3f). Exported FIO-agents predominantly entered the stream via seepage from degraded soil (Figure 9d) as simulated overland flow was limited (Figure 5). When overland flow did transfer FIO-agents to the stream, localised spikes in export fluxes were simulated (Figure 9c-d). Contributions were non-linear due to the changing storage of FIO-agents. When cattle were in Mid Pasture (R), both seepage and direct deposition made their greatest contributions of FIO-agents to the stream (Figures 3f and 9d), reflecting the higher loading rates of *E. coli* from cattle (see Table 4 in Neill et al., *in review*) and the extensive stream access in this field (Figure 1c). Variability in flux magnitudes between ensemble runs was also greatest at this time (Figure 9c). Contributions from direct deposition were otherwise minimal, reflecting the lower loading rates of sheep (see Table 4 in Neill et al., *in review*) when present in Mid Pasture (R) or the limited number of discrete crossing points allowing stream access to livestock in other fields (Figures 1c and 3e). Contributions from different livestock types largely corresponded to their presence in the catchment (Figures 3f and 9e); however, a limited "memory-effect" in contributions reflected survival of FIO-agents in areas of degraded soil.

Over the MOP, similar median numbers of exported FIO-agents entered the stream via direct deposition wherever livestock were present with stream access (Figures 1c, 3f and 10a). However, stochastic variability across the ensemble runs was evident (Figure 10b). Pathways taken by exported FIO-agents reaching the stream in overland flow or seepage were constrained by the limited area over which the former was generated in the catchment (Figures 5 and 10c). Fluxes of exported FIO-agents along individual pathways increased towards the stream with generation of overland flow (Figures 5b and 10c); however, short pathways between areas of degraded soil and the stream were consistently followed by the largest numbers of exported FIO-agents (Figures 1c and 10c). Overall, source areas contributing exported FIO-agents to the stream over the MOP were always restricted to stream-proximal locations (Figure 10c-d). Stochastic variability in numbers of exported FIO-agents following particular pathways to the stream was usually less than for numbers being directly deposited in the stream (Figure 10b and d).

On the example dry and wet days, there was a difference in the spatial distribution of cells for which the median number of exported FIO-agents entering the stream via direct deposition was non-zero (Figure 11a and c). However, similar counts of sheep in Lower Pasture (L) and Mid Pasture (R) on both days (Figure 3f) meant that when non-zero, median numbers were comparable (Figure 11a and c). In addition, stochastic variability across ensemble runs showed that on either day, direct deposition of exported FIO-agents could occur wherever livestock had stream access (Figure 11b and d). More extensive overland flow on the wet day (Figure 6b) increased the spatial extent of pathways taken by exported FIO-agents to the stream, although contributing areas were always limited to near-stream locations (Figure 11e and g). Fluxes of FIO-agents along individual pathways were elevated in wet conditions (Figure 11g) due to the increased generation of overland flow (Figure 6b). For both the dry and wet days, "average" maps indicated pathways taken by exported FIO-agents to the stream (Figure 11e and g) that fully consisted of cells where overland flow was simulated (Figure 6b) or seepage from degraded soil was possible (Figure 1c). However, from considering the effect of stochastic variability between ensemble simulations (Figure 11f and h), it is apparent that in some instances, exported FIO-agents had followed paths that included cells not hydrologically connected to the stream during the timestep in question (e.g. in Lower Pasture [L]; Figures 1c and 6b). This indicates that FIO-agents previously moved and infiltrated into the soil could be exfiltrated and further transported. Stochastic variability in numbers of exported FIO-agents following particular pathways to the stream was generally lower overall for the dry event (Figure 11f and h).

5. Discussion

5.1 To what extent does MAFIO resolve the main processes driving observed FIO dynamics?

Using models to explore issues of water quality, especially in a decision-making context, requires confidence that processes governing the determinand of interest are adequately captured (c.f. Vaché and McDonnell, 2006; Wellen et al., 2015). Consequently, the new agent-based model MAFIO was applied to the Tulloch Burn for a relatively data-rich period, in order to assess the adequacy of process representation in the model. The spatially-distributed, tracer-aided ecohydrological model EcH_2O-iso provided the hydrological environment to improve confidence in the robustness of simulated hydrological processes underpinning FIO simulations (c.f. Birkel and Soulsby, 2015; Neill et al., 2019). However, whilst multi-criteria calibration to discharge and isotope data allowed elements of catchment hydrological functioning to be reasonably constrained (i.e. dominance of groundwater, generation of overland flow proximal to the stream), uncertainty persisted in the exact spatial extent of overland flow paths (Figure 7c). This can obscure whether deficiencies in FIO simulations arise from uncertainty in simulated hydrology or the need to refine process conceptualisation in MAFIO; where this may be an issue is highlighted in the discussion that follows. This also necessitates that a full quantitative

uncertainty analysis be the subject of future work (c.f. Beven and Lamb, 2017), and reinforces the need for collection of diverse datasets for use in constraining highly-parametrised models (Kelleher et al., 2017; Kuppel et al., 2018b).

The consistent simulation of zero loads of *E. coli* at T8 despite non-zero loads being observed likely indicates that process conceptualisation in MAFIO itself requires refinement (Figure 8e). This assertion arises from confidence in the lack of surface connectivity between T8 and Top Pasture (the only upstream source of livestock-derived FIOs) simulated by the "best" run of EcH_2O-iso (Figure 5b), despite the overall uncertainty in the exact extent of overland flow paths (Figure 7c). Specifically, the skill of this run in capturing observed isotope dynamics at T8 (Figure 4j) indicates that no overland flow upstream of this site is plausible. Furthermore, increased tree water use in the forest separating T8 and Top Pasture (Douinot et al., 2019) combined with likely enhanced filtering of FIOs in overland flow by the forest floor (Kay et al., 2012) suggests limited opportunities for surface transport of FIOs between these locations. Given that deer and hares have been observed in the forest around T8, a possible refinement to MAFIO could be inclusion of wild animals as sources of FIOs. Indeed, wildlife (including gastropods, frogs and fish as previously unrecognised sources; Frick et al., 2018) have previously been found to significantly impact microbial water quality, even in agricultural areas (Muirhead et al., 2011). An alternative refinement could be accounting for possible sources of "naturalised" FIOs that have adapted to persist and grow in the environment (e.g. Jang et al., 2017). A key issue to consider when conceptualising the former would be the increased uncertainty in loading and die-off parameters associated with FIOs from wildlife (Guber et al., 2015). Furthermore, difficulties also exist in characterising population levels and movement of wild animals in the landscape (Tetzlaff et al., 2010). This latter issue could likely be overcome by representing wildlife movements stochastically in MAFIO. Whilst this would probably result in greater stochastic variability across ensemble simulations, it would help increase confidence that the potential impacts of wildlife as a source of FIOs are being represented.

This last point is relevant when inferring process adequacy from the large spread in non-zero loads simulated at T6 (Figure 8c-d). As there were again no surface flow paths upstream of this site in the simulated hydrological environment (Figure 5b), FIO-agents could only be directly deposited in the stream by livestock in Mid Pasture (R). Given the stochastic treatment of livestock movement and, consequently, direct deposition in MAFIO, it should be expected that different ensemble runs will collectively simulate a range of possible *E. coli* loads dependent on when and where livestock were simulated to directly defecate in the stream (c.f. Abdou et al., 2012). Given the plausibility of direct deposition influencing microbial water quality at T6 when livestock are present in Mid Pasture (R) due to stream accessibility (Figure 1c), observed loads may reflect one particular realisation of how

livestock entered the stream and directly deposited (c.f. Windrum et al., 2007). Consequently, that observations could fall within the spread of simulated loads (Figure 8c-d) likely suggests that MAFIO is adequately representing the process of direct deposition. Thus, it cannot be concluded that the large spread in simulated non-zero loads is indicative of model inadequacy (c.f. Parker and Meretsky, 2004).

A more problematic feature of simulations at T6 is the consistent simulation of zero loads when livestock were absent from Mid Pasture (R) despite observed non-zero loads (Figures 3f and 8c). This could reflect incorrect simulation of zero loads at T8, depending on the extent to which upstream locations influence microbial water quality at T6 (Neill et al., 2018; Vitro et al., 2017). Qualitative similarity between observed *E. coli* dynamics at T6 and T8 when livestock were absent from Mid Pasture (R) lends some support to this possibility (Figures 3c-d and f). However, uncertainty in the exact spatial extent of flow paths simulated by EcH_2O-iso also means that surface connectivity between Mid Pasture (R) and the stream could have plausibly been simulated by some behavioural model runs. Such connectivity could facilitate transfer of FIOs to the stream in the absence of livestock, depending on longevity of survival (Martinez et al., 2013). Consequently, further work to reduce uncertainty in simulated flow paths is necessary to determine whether under-predictions at T6 have a hydrological or microbiological cause. A further possibility could be that a streambed reservoir of *E. coli* from livestock in Mid Pasture (R) exists that can be mobilised by streamflow (McDonald et al., 1982). However, this mechanism would be unlikely to explain under-predictions that occurred during times of recessional and base flows (Figures 3a and 8c; Nagels et al., 2002).

Despite the tendency to over-estimate loads in absolute terms, MAFIO had most skill in capturing observed *E. coli* dynamics at the outlet (Figure 8a-b). Furthermore, stochastic variability in simulations was reduced compared to T6 (Figure 8a-d). Combined, these results suggest that potential process deficiencies impacting upstream sites had less influence here. This likely reflected greater opportunities for FIO-agents to reach the stream via seepage and transport in overland flow generated by areas proximal to the stream in the lower catchment (Figures 1c, 5 and 9). The promising performance at the outlet suggests the model reasonably well-captures these highly-localised mechanisms of FIO transfer as dominant drivers of impaired microbial water quality at this location. This is further supported by relative confidence in EcH_2O-iso simulations of overland flow generation close to the stream and spatial patterns of soil saturation deficit underpinning seepage (Figure 7a and d) and would be consistent with the likely importance of localised sources of FIOs in the wider Tarland Burn (Neill et al., 2018). The over-estimation of loads at the outlet, however, highlights there is scope for improving the degree to which simulations capture the detail in observations. Consequently, several avenues for model

refinement are identified that may help increase correspondence between observed and simulated loads at the outlet and lead to more nuanced simulation of general FIO dynamics.

Many parameters relating to the loading, die-off, and transport of FIOs are characterised by uncertainty (Cho et al., 2016). Therefore, in addition to a quantitative assessment of how flow path uncertainty in EcH_2O-iso affects MAFIO simulations, a sensitivity analysis and calibration of MAFIO parameters should also be conducted. This may help better-constrain parameters and improve simulations whilst enhancing understanding of how parameter uncertainty is propagated into model outputs (e.g. Beven, 2006). However, limitations in using "fit-to-data" metrics to assess ABM performance likely means that alternative automated calibration procedures will need developing (c.f. Polhill and Salt, 2017). MAFIO has also been applied at relatively coarse spatial (30×30 m) and temporal (1-day timestep) resolutions in this initial application. Whilst this spatial scale is finer than permitted by most process-based FIO models (e.g. Dorner et al., 2006; Whitehead et al., 2016), resolving non-linearities in the fate and transport of FIOs arising from the effects of small-scale heterogenity in the landscape (e.g. micro-topography influencing flow paths; Frei et al., 2010) or processes operating at sub-daily timescales (e.g. intra-storm precipitation dynamics; McKergow and Davies-Colley, 2010) may be necessary for more nuanced simulation of FIO dynamics. Finally, alternative methods of allowing MAFIO to simulate the large populations of FIOs found in catchments could be trialled. One possibility is use of "super-individuals" (Scheffer et al., 1995). Like FIO-agents, these are introduced into a simulation for every given number of real individuals. However, this number is then assigned to the super-individual as an attribute that is influenced by controlling processes, which may give a more complete simulation of dynamics that would be observed if all individuals were represented explicitly (Scheffer et al., 1995). Exploring these avenues for model refinement will be a focus of future work.

5.2 What potential does MAFIO have for providing process-based insights into microbial water quality that are relevant for management?

The preceding discussion highlights the status of MAFIO as a research-level model. However, application to Tulloch Burn still provided insight into how an agent-based approach has significant potential for identifying drivers of microbial water quality at scales relevant for management.

Management of microbial water quality at the farm scale is always likely to have financial implications for the farmer (Oliver et al., 2007). Consequently, information aiding spatial targeting of cost-effective and efficient mitigation measures is desirable (c.f. Oliver et al., 2018, Vinten et al., 2017). The facility to interrogate the *Domain type* and *Location memory* attributes of exported FIO-agents in MAFIO

permits insights into the transfer mechanisms and source areas contributing FIOs to streams, which may have significant value in this respect. For the Tulloch Burn, for example, it was revealed that whilst overland flow could cause spikes in the flux of exported FIO-agents during events, its limited capacity to transport FIO-agents to the stream in both time and space meant that seepage from areas of degraded soil was always the dominant transfer mechanism (Figures 9-11). Overall, this led to exported FIO-agents being sourced from locations highly proximal to the stream under all conditions (Figures 10-11). As the skill of MAFIO in simulating observed *E. coli* dynamics at the outlet suggests these localised mechanisms are dominant drivers of microbial water quality (Figure 8a-b), an implication is that small-scale interventions (e.g. building bridges between fields separated by the stream or preventing livestock access to stream-proximal locations capable of generating overland flow) could result in significant improvements to microbial water quality without the need for larger-scale and more costly measures (e.g. reducing stocking densities or extensive use of buffer strips; Cuttle et al., 2006).

Quantitative microbial risk assessment (QMRA) can further assist in selection of mitigation measures by providing a basis for assessing how risks presented by faecal pathogens to human health can be reduced through management (Haas et al., 2014; Strachan et al., 2005). Usually, a dose-response model estimates the likelihood of an adverse health effect occurring based on an input dosage of pathogens (Haas et al., 2014). Direct quantification of pathogens in water is not common, however, due to their lower occurrence with respect to FIOs and the costly methods necessary for their enumeration (Geldreich, 1996). Therefore, it may be necessary to estimate exposure based on the prevalence of pathogens in animals responsible for contaminating the medium humans come into contact with (c.f. Strachan et al., 2002). In this regard, MAFIO simulations attributing contributions of exported FIO-agents to different livestock types (Figure 9e) could prove useful. Furthermore, the agent-based model structure could allow direct simulation of pathogenic organisms alongside non-pathogenic FIOs, subject to sufficient data availability to inform parameterisations or rule sets associated with pathogenic FIO-agents (c.f. Hipsey et al., 2008).

A characteristic of MAFIO which also has potential management value is the ability to model processes stochastically. This can enable greater representation of how both natural variability and uncertainty in simulated processes propagate to predictions of microbial water quality, which may be useful for decision making (c.f. Brouwer and De Blois, 2008). Indeed, application of MAFIO to the Tulloch Burn highlighted how simulated *E. coli* loads may demonstrate considerable spread due to variability and uncertainty in how livestock use the landscape and, consequently, directly defecate in streams (c.f. Oliver et al., 2010). However, full realisation of this value would be contingent on the development of

733 appropriate calibration methods for ABMs which quantify how parameter and structural uncertainty
734 also propagate to model outputs, as discussed earlier.

735

736 A final important point relates to the data requirements of MAFIO and its consequent transferability.
737 As previously highlighted, availability of diverse observations corresponding to model outputs will
738 benefit calibration / validation of the model and its associated hydrological environment simulator (c.f.
739 Kelleher et al., 2017; Kuppel et al., 2018b). However, where such observations exist, it is not necessary
740 that model inputs be derived from site-specific data such as those available in this study following
741 intensive monitoring at the Tulloch Burn. For example, nationally-available datasets combined with
742 simple assumptions regarding grazing practices could provide the spatial arrangement of fields within
743 a catchment along with livestock counts that vary in space and time (e.g. Oliver et al., 2010, 2018).
744 Furthermore, use of local datasets (e.g. regarding stream fencing as in Dymond et al., 2016) alongside
745 one-off farm surveys or farmer interviews (Oliver et al., 2007, 2009) could sufficiently characterise the
746 spatial distributions of stream accessibility to livestock and areas of degraded soil. Other necessary
747 catchment characteristics can be derived from widely-available data (e.g. elevation, soil types, etc.)
748 integrated into a geographical information system. Finally, where site-specific data on FIO
749 concentrations in faeces and soil are unavailable, estimates may be derived from literature values (e.g.
750 Dorner et al., 2006; Hipsey et al., 2008; Whitehead et al., 2016). Consequently, it should be possible to
751 apply MAFIO to less intensively-studied catchments. It is also important to emphasise that any
752 hydrological model could be used to provide the hydrological environment for MAFIO as long as its
753 consistency with catchment hydrological functioning can be robustly assessed.

754

755 ## 6. Conclusions

756 This work provided a proof-of-concept application for MAFIO, an agent-based model designed to
757 unravel the spatio-temporal dynamics of sources and transfer mechanisms contributing FIOs to streams
758 at the sub-field scale. Performance in simulating observed *E. coli* dynamics in the Tulloch Burn
759 catchment showed that the model has skill in capturing the transfer of FIOs from livestock to streams
760 via the processes of direct deposition, overland flow and seepage from areas of degraded soil. This
761 assessment was aided by EcH_2O-iso, the hydrological environment simulator for MAFIO, identifying
762 generation of overland flow close to the stream and dominance of groundwater in the catchment with
763 some confidence following multi-criteria calibration to discharge and isotope data. However,
764 uncertainty in the exact spatial extent of overland flow paths simulated by EcH_2O-iso meant it was not
765 always clear whether deficiencies in MAFIO performance reflected a hydrological or microbiological
766 cause. This identified the need for a quantitative assessment of uncertainty propagation from EcH_2O-

767 iso to MAFIO to be the subject of future work. Nonetheless, under-prediction of observed *E. coli* loads
768 in the upper catchment implied the need to consider "naturalised" or wildlife sources of FIOs in the
769 model, and it was further possible to identify several avenues relating to issues of scale and calibration
770 that could be explored to improve model performance.

771

772 Despite the present status of MAFIO as a research-level model, this application revealed how the agent-
773 based structure of the model allowed it to have significant potential for informing management.
774 Interrogation of the attributes of FIO-agents exported from the catchment could reveal insights into
775 source areas, transfer mechanisms and livestock contributing FIOs to the stream, providing information
776 that could inform implementation of efficient, cost-effective mitigation measures. Furthermore, the
777 potential to model processes stochastically in MAFIO allowed the effects of natural variability and
778 uncertainty in processes influencing microbial water quality to be characterised, which may have value
779 in a decision support context. Whilst this proof-of-concept study identified possible refinements that
780 could be made to MAFIO, once addressed, it is likely that the model could have substantial value in
781 underpinning decision support frameworks aimed at mitigating impaired microbial water quality.

782

783 **Software and data availability**

784 The source code for MAFIO as used in this work is available via the University of Aberdeen PURE
785 repository: https://doi.org/10.20392/66f74663-ece3-4a52-8bed-f0cf52d0831a.

786 The source code for EcH_2O-iso is available at: https://bitbucket.org/sylka/ech2o_iso/src/master_2.0/.

787 The Tulloch Burn datasets used in this study are available from the lead author on request.

788

789 **Acknowledgments**

790 Funding for this work from the Scottish Government's Hydro Nation Scholars Programme is gratefully
791 acknowledged. Many thanks to Audrey Innes, Jonathan Dick, Claire Tunaley and Bernhard Scheliga
792 for their assistance in analysing the isotope samples. In addition, thanks to Allan Sim, Duncan White
793 and, in particular, Claire Abel and Adam Wyness for instruction and training on microbiological
794 sampling and analysis techniques. Simulations with EcH_2O-iso and MAFIO were undertaken on the
795 Maxwell high performance computing cluster funded by the University of Aberdeen. Sylvain Kuppel
796 and Aaron Smith are thanked for their assistance in troubleshooting occasional issues with EcH_2O-iso.

797

References

Abdou, M., Hamill, L., Gilbert, N., 2012. Designing and Building an Agent-Based Model: 141-166 in Heppenstall, A.J., Crooks, A.T., See, L.M., Batty, M. (eds). Agent-Based Models of Geographical Systems. Springer: Dordrecht, Heidelberg, London, New York.

Ala-aho, P., Tetzlaff, D., McNamara, J.P., Laudon, H., Soulsby, C., 2017. Using isotopes to constrain water flux and age estimates in snow-influenced catchments using the STARR (Spatially distributed Tracer-Aided Rainfall-Runoff) model. Hydrological Earth Systems Science 21, 5089-5110.

Bergfur, J., Demars, B.O.L., Stutter, M.I., Langan, S.J., Friberg, N., 2012. The Tarland Catchment Initiative and Its Effect on Stream Water Quality and Macroinvertebrate Indices. Journal of Environmental Quality 41: 314-321.

Beven, K., 2006. A manifesto for the equifinality thesis. Journal of Hydrology 320, 18-36.

Beven, K., 2012. Rainfall-runoff Modelling: The Primer (Second Edition). John Wiley and Sons: Chichester, UK.

Beven, K., 2019. Towards a methodology for testing models as hypotheses in the inexact sciences. Proceedings of the Royal Society A 475: 20180862.

Beven, K., Lamb, R., 2017. The uncertainty cascade in model fusion. Geological Society, London, Special Publications 408: 255-266.

Bilotta, G.S., Brazier, R.E., Haygarth, P.M., 2007. The impacts of grazing animals on the quality of soils, vegetation and surface waters in intensively managed grasslands. Advances in Agronomy 94: 237-280.

Birkel, C., Soulsby, C., 2015. Advancing tracer-aided rainfall-runoff modelling: a review of progress, problems and unrealised potential. Hydrological Processes 29: 5227-5240.

Brouwer, R., De Blois, C., 2008. Integrated modelling of risk and uncertainty underlying the cost and effectiveness of water quality measures. Environmental Modelling and Software 23: 922-937.

Brown, D.G., Page, S., Riolo, R., Zellner, M., Rand, W., 2005. Path dependence and the validation of agent-based spatial models of land use. International Journal of Geographical Information Science 19: 153-174.

Cho, K.H., Pachepsky, Y.A., Oliver, D.M., Muirhead, R.W., Park, Y., Quilliam, R.S., Shelton, D.R., 2016. Modelling fate and transport of fecally-derived microorganisms at the watershed scale: State of the science and future opportunities. Water Research 100: 38-56.

825 Cuttle, S.P., Macleod, C.J.A., Chadwick, D.R., Scholefield, D., Haygarth, P.M., Newell-Price, P., Harris, D.,
826 Shepherd, M.A., Chambers, B.J., Humphrey, R., 2006. An inventory of methods to control diffuse water
827 pollution from agriculture (DWPA): User Manual. Accessed July 2019 from
828 http://randd.defra.gov.uk/Document.aspx?Document=es0203_4145_FRA.pdf

829 Dee, D.P., Uppala, S.M., Simmons, A.J., Berrisford, P., Poli, P., Kobayashi, S., Andrae, U., Balmaseda, M.A.,
830 Balsamo, G., Bauer, P., Bechtold, P., Beljaars, A.C.M., van de Berg, L., Bidlot, J., Bormann, N., Delsol,
831 C., Dragani, R., Fuentes, M., Geer, A.J., Haimberger, L., Healy, S.B., Hersbach, H., Holm, E.V., Isaksen,
832 L., Kållberg, P., Kohler, M., Matricardi, M., McNally, A.P., Monge-Sanz, B.M., Morcrette, J.-J., Park,
833 B.-K., Peubey, C., de Rosnay, P., Tavolato, C., Thepaut, J.-N., Vitart, F., 2011. The ERA-Interim
834 reanalysis: configuration and performance of the data assimilation system. Quarterly Journal of the Royal
835 Meteorological Society 137: 553-597.

836 Dorner, S.M., Anderson, W.B., Slawson, R.M., Kouwen, N., Huck, P.M., 2006. Hydrologic modeling of pathogen
837 fate and transport. Environmental Science and Technology 40, 4746-4753.

838 Douinot, A., Tetzlaff, D., Maneta, M., Kuppel, S., Schulte-Bisping, H., Soulsby, C., 2019. Ecohydrological
839 modelling with EcH_2O-iso to quantify forest and grassland effects of water partitioning and flux ages.
840 Hydrological Processes 33: 2174-2191.

841 Dunn, S.M., Johnston, L., Taylor, C., Watson, H., Cook, Y., Langan, S.J., 2013. Capability and limitations of a
842 simple grid-based model for simulating land use influences on stream nitrate concentrations. Journal of
843 Hydrology 507: 110-123.

844 Dymond, J.R., Serezat, D., Ausseil, A.G.E., Muirhead, R.W., 2016. Mapping of Escherichia coli sources
845 connected to waterways in the Ruamahanga catchment, New Zealand. Environmental Science and
846 Technology 50(4), 1897-1905.

847 Frei, S., Lischeid, G., Fleckenstein, J.H., 2010. Effects of micro-topography on surface–subsurface exchange and
848 runoff generation in a virtual riparian wetland – A modeling study. Advances in Water Resources 13(11),
849 1388–1401.

850 Frick, C., Vierheilig, J., Linke, R., Savio, D., Zornig, H., Antensteiner, R., Baumgartner, C., Bucher, C., Blaschke,
851 A.P., Derx, J., Kirschner, A.K.T., Ryzinska-Paier, G., Mayer, R., Seidl, D., Nadiotis-Tsaka, T., Sommer,
852 R., Farnleitner, A.H., 2018. Poikilothermic Animals as a Previously Unrecognized Source of Fecal
853 Indicator Bacteria in a Backwater Ecosystem of a Large River. Applied and Environmental Microbiology
854 84: e00715-18.

855 Geldreich, E.E., 1996. Pathogenic agents in freshwater resources. Hydrological Processes 10: 315-333.

856 Goody, R.M., Yung, Y.L., 1995. Atmospheric Radiation: Theoretical Basis. Oxford University Press: Oxford,
857 UK.

858 Greene, S., Johnes, P.J., Bloomfield, J.P., Reaney, S.M., Lawley, R., Elkhatib, Y., Freer, J., Odoni, N., Macleod,
859 C.J.A., Percy, B., 2015. A geospatial framework to support integrated biogeochemical modelling in the
860 United Kingdom. Environmental Modelling and Software 68: 219-232.

861 Guber, A.K., Fry, J., Ives, R.L., Rose, J.B., 2015. Escherichia coli Survival in, and release from, White-Tailed
862 Deer feces. Applied and Environmental Microbiology 81, 1168-1176.

863 Gupta, H.V., Kling, H., Yilmaz, K.K., Martinez, G.F., 2009. Decomposition of the mean squared error and NSE
864 performance criteria: Implications for improving hydrological modelling. Journal of Hydrology 377: 80-
865 91.

866 Hannaford, J., Muchan, K., Lewis, M., Clemas, S., 2018. Hydrological summary for the United Kingdom:
867 December 2017. Wallingford, UK: NERC/Centre for Ecology & Hydrology. Accessed June 2019 from
868 http://nora.nerc.ac.uk/id/eprint/518984/

869 Haas, C.N., Rose, J.B., Gerba, C.P., 2014. Quantitative microbial risk assessment (Second Edition). Wiley:
870 Hoboken, New Jersey.

871 Haydon, S., Deletic, A., 2006. Development of a coupled pathogen-hydrologic catchment model. Journal of
872 Hydrology 328: 467-480.

873 Hipsey, M.R., Antenucci, J.P., Brookes, J.D., 2008. A generic, process-based model of microbial pollution in
874 aquatic systems. Water Resources Research 44, W07408.

875 Hrachowitz, M., Soulsby, C., Tetzlaff, D., Speed, M., 2010. Catchment transit times and landscape controls—
876 does scale matter? Hydrological Processes 24: 117–125.

877 Jang, J., Hur, H.-G., Sadowsky, M.J., Byappanahalli, M.N., Yan, T., Ishii, S., 2017. Environmental Escherichia
878 coli: ecology and public health implications—a review. Journal of Applied Microbiology 123: 570-581.

879 Kay, D., Crowther, J., Kay, C., Mcdonald, A.T., Ferguson, C., Stapleton, C.M., Wyer, M.D., 2012. Effectiveness
880 of best management practices for attenuating the transport of livestock-derived pathogens within
881 catchments: 195-255 in Dufour, A., Bartram, J., Bos, R., Gannon, V. (eds.). Animal waste, water quality
882 and human health. IWA Publishing: London.

Kay, D., Crowther, J., Stapleton, C.M., Wyer, M.D., Fewtrell, L., Anthony, S., Bradford, M., Edwards, A., Francis, C.A., Hopkins, M., Kay, C., McDonald, A.T., Watkins, J., Wilkinson, J., 2008. Faecal indicator organism concentrations and catchment export coefficients in the UK. Water Research 42: 2649-2661.

Kelleher, C., McGlynn, B., Wagener, T., 2017. Characterising and reducing equifinality by constraining a distributed catchment model with regional signatures., local observations and process understanding. Hydrology and Earth Systems Science 21: 3325-3352.

Krause, P., Boyle, D.P., Bäse, F., 2005. Comparison of different efficiency criteria for hydrological model assessment. Advances in Geosciences 5: 89-97.

Kuppel, S., Tetzlaff, D., Maneta, M.P., Soulsby, C., 2018a. EcH2O-iso 1.0: water isotopes and age tracking in a process-based, distributed ecohydrological model. Geoscientific Model Development 11: 3045-3069.

Kuppel, S., Tetzlaff, D., Maneta, M.P., Soulsby, C., 2018b. What can we learn from multi-criteria calibration of a process-based ecohydrological model? Environmental Modelling and Software 101: 301-316.

Langan, S.J., Wade, A.J., Smart, R.P., Edwards, A.C., Soulsby, C., Billett, M.F., Jarvie, H.P., Cresser, M.S., Owen, R., Ferrier, R.C., 1997. The prediction and management of water quality in a relatively unpolluted major Scottish catchment: current issues and experimental approaches. Science of the Total Environment 194-195: 419-435.

Legates, D.R., McCabe, G.J., 1999. Evaluating the use of "goodness-of-fit" measures in hydrologic and hydroclimatic model validation. Water Resources Research 35: 233-241.

Martinez, G., Pachepsky, Y.A., Shelton, D.R., Whelan, G., Zepp, R., Molina, M., Panhorst, K., 2013. Using the Q_{10} model to simulate *E. coli* survival in cowpats on grazing lands. Environmental International 54: 1-10.

McDonald, A., Kay, D., Jenkins, A., 1982. Generation of fecal and total coliform surges by stream flow manipulation in the absence of normal hydrometeorological stimuli. Applied and Environmental Microbiology 44: 292-300.

McKergow, L.A., Davies-Colley, R.J., 2010. Stormflow dynamics and loads of *Escherichia coli* in a large mixed land use catchment. Hydrological Processes 24: 276-289.

Morris, M.D., 1991. Factorial sampling plans for preliminary computational experiments. Technometrics 33: 161-174.

911 Moss, S., Edmonds, B., 2005. Sociology and Simulation: Statistical and Qualitative Cross-Validation. American
912 Journal of Sociology 110: 1095-1131.

913 Muirhead, R.W., 2009. Soil and faecal material reservoirs of Escherichia coli in a grazed pasture, New Zealand
914 Journal of Agricultural Research 52: 1-8.

915 Muirhead, R.W., Elliot, A.H., Monaghan, R.M., 2011. A model framework to assess the effect of dairy farms and
916 wild fowl on microbial water quality during base-flow. Water Research 45: 2863–2874.

917 Nagels, J.W., Davies-Colley, R.J., Donnison, A.M., Muirhead, R.W., 2002. Faecal contamination over flood
918 events in a pastoral agricultural stream in New Zealand. Water Science and Technology 45: 45-52.

919 Neill, A.J., Tetzlaff, D., Strachan, N.J.C., Soulsby, C., 2019. To what extent does hydrological connectivity
920 control dynamics of faecal indicator organisms in streams? Initial hypothesis testing using a tracer-aided
921 model. Journal of Hydrology 570: 423-435.

922 Neill, A.J., Tetzlaff, D., Strachan, N.J.C., Hough, R.L., Avery, L.M., Watson, H., Soulsby, C., 2018. Using spatial-
923 stream-network models and long-term data to understand and predict dynamics of faecal contamination
924 in a mixed land-use catchment. Science of the Total Environment 612: 840-852.

925 Neill, A.J., Tetzlaff, D., Strachan, N.J.C., Hough, R.L., Avery, L.M., Kuppel, S., Maneta, M.P., Soulsby, C., *in*
926 *review*. An agent-based model that simulates the spatio-temporal dynamics of sources and transfer
927 mechanisms contributing faecal indicator organisms to streams. Part 1: Background and model
928 description. Journal of Environmental Management.

929 O'Sullivan, D., Millington, J., Perry, G. & Wainwright, J., 2012. Agent-based models – because they're worth it?:
930 109-123 in Heppenstall, A.J., Crooks, A.T., See, L.M., Batty, M. (eds). Agent-Based Models of
931 Geographical Systems. Springer: Dordrecht, Heidelberg, London, New York.

932 Oliver, D.M., Heathwaite, A.L., Hodgson, C.J., Chadwick, D.R., 2007. Mitigation and current management
933 attempts to limit pathogen survival and movement within farmed grassland. Advances in Agronomy 93:
934 95-152.

935 Oliver, D.M., Bartie, P.J., Heathwaite, A.L., Reaney, S.M., Parnell, J.A.Q., Quilliam, R.S., 2018. A catchment-
936 scale model to predict spatial and temporal burden of *E. coli* on pasture from grazing livestock. Science
937 of the Total Environment 616-617: 678-687.

938 Oliver, D.M., Fish, R.D., Hodgson, C.J., Heathwaite, A.L., Chadwick, D.R., Winter, M., 2009. A cross-
939 disciplinary toolkit to assess the risk of faecal indicator loss from grassland farm systems to surface
940 waters. Agriculture, Ecosystems and Environment 129: 401-412.

941 Oliver, D.M., Page, T., Hodgson, C.J., Heathwaite, A.L., Chadwick, D.R., Fish, R.D., Winter, M., 2010.
942 Development and testing of a risk indexing framework to determine field-scale critical source areas of
943 faecal bacteria on grassland. Environmental Modelling and Software 25: 503-512.

944 Oliver, D.M., Porter, K.D.H., Pachepsky, Y.A., Muirhead, R.W., Reaney, S.M., Coeffey, R., Kay, D., Milledge,
945 D.G., Hong, E., Anthony, S.G., Page, T., Bloodworth, J.W., Mellander, P., Carbonneau, P., McGrane,
946 S.J., Quilliam, R.S., 2016. Predicting microbial water quality with models: Over-arching questions for
947 managing risk in agricultural catchments. Science of the Total Environment 544: 39-47.

948 Parker, D.C., Meretsky, V., 2004. Measuring pattern outcomes in an agent-based model of edge-effect
949 externalities using spatial metrics. Agriculture, Ecosystems and Environment 101: 233-250.

950 Parry, H.R., Bithell, M., 2012. Large scale agent-based modelling: A review and guidelines for model scaling:
951 271-308 in Heppenstall, A.J., Crooks, A.T., See, L.M., Batty, M. (eds). Agent-Based Models of
952 Geographical Systems. Springer: Dordrecht, Heidelberg, London, New York.

953 Polhill, J.G., Sutherland, L., Gotts, N.M., 2010. Using qualitative evidence to enhance and agent-based modelling
954 system for studying land use change. Journal of Artificial Societies and Social Simulation 13 (2) 10.
955 http://jasss.soc.surrey.ac.uk/13/2/10.html

956 Polhill, J.G., Salt, D., 2017. The importance of ontological structure: why validation by 'fit-to-data' is insufficient:
957 141-172 in Edmonds, B., Meyer, R. (eds.) Simulating Social Complexity: A Handbook (Second Edition).
958 Springer: Dordrecht, Heidelberg, London, New York.

959 Porter, K.D.H., Reaney, S.M., Quilliam, R.S., Burgess, C., Oliver, D.M., 2017. Predicting diffuse microbial
960 pollution risk across catchments: The performance of SCIMAP and recommendations for future
961 development. Science of the Total Environment 609: 456-465.

962 Reaney, S.M., 2008. The use of agent based modelling techniques in hydrology: determining the spatial and
963 temporal origin of channel flow in semi-arid catchments. Earth Surface Processes and Landforms 33,
964 317-327.

965 Refsgaard, J.C., van der Sluijs, J.P., Højberg, A.L., Vanrolleghem, P.A., 2007. Uncertainty in the environmental
966 modelling process – A framework and guidance. Environmental Modelling and Software 22: 1543-1556.

967 Rode, M., Arhonditsis, G., Balin, D., Kebede, T., Krysanova, V., van Griensven, A., van der Zee, S.E.A.T.M.,
968 2010. New challenges in integrated water quality modelling. Hydrological Processes 24: 3447-3461.

969 Sadeghi, A., Arnold, J., 2002. A SWAT/Microbial Sub-Model for Predicting Pathogen Loadings in Surface and
970 Groundwater at Watershed and Basin Scales. In Total Maximum Daily Load (TMDL): Environmental
971 Regulations, Proceedings of 2002 Conference (p. 56). American Society of Agricultural and Biological
972 Engineers.

973 Schaefli, B., Gupta, H.V., 2007. Do Nash values have value? Hydrological Processes 21: 2075-2080.

974 Scheffer, M., Baveco, J.M., DeAndelis, D.L., Rose, K.A., van Nes, E.H., 1995. Super-individuals a simple
975 solution for modelling large populations on an individual basis. Ecological Modelling 80: 161-170.

976 Soheir, H., Farges, J-L., Piet-Lahanier, H., 2014. Improvement of the representativity of the Morris Method for
977 air-launch-to-orbit separation. IFAC Proceedings Volumes 47(3): 7954-7959.

978 Soil Survey of Scotland Staff, 2014. Digitized soil map of Scotland, scale 1:25 000. James Hutton Institute.

979 Sprenger, M., Stumpp, C., Weiler, M., Aeschbach, W., Allen, S.T., Benettin, P., Dubbert, M., Hartmann, A.,
980 Hrachowitz, M., Kirchner, J.W., McDonnell, J.J., Orlowski, N., Penna, D., Pfahl, S., Rinderer, M.,
981 Rodriguez, N., Schmidt, M., Werner, C., 2019. The demographics of water: A review of water ages in
982 the critical zone. Reviews of Geophysics 57: 800-834.

983 Strachan, N.J.C., Dunn, G.M., Ogden, I.D., 2002. Quantitative risk assessment of human infection from
984 *Escherichia coli* O157 associated with recreational use of animal pasture. International Journal of Food
985 Microbiology 75: 39-51.

986 Strachan, N.J.C., Doyle, M.P., Kasuga, F., Rotariu, O., Ogden, I.D., 2005. Dose response modelling of
987 *Escherichia coli* O157 incorporating data from foodborne and environmental outbreaks. International
988 Journal of Food Microbiology 103: 35-47.

989 Tetzlaff, D., Soulsby, C., Birkel, C., 2010. Hydrological connectivity and microbiological fluxes in montane
990 catchments: the role of seasonality and climatic variability. Hydrological Processes 24: 1231-1235.

991 Vaché, K.B., McDonnell, J.J., 2006. A process-based rejectionist framework for evaluating catchment runoff
992 model structure. Water Resources Research 42, W02409.

993 Vinten, A., Sample, J., Ibiyemi, A., Abdul-Salam, Y., Stutter,M., 2017. A tool for cost-effectiveness analysis of
994 field scale sediment-bound phosphorus mitigation measures and application to analysis of spatial and

temporal targeting in the Lunan Water catchment, Scotland. Science of the Total Environment 586: 631–641.

Vitro, K.A., BenDor, T.K., Jordanova, T.V., Miles, B., 2017. A geospatial analysis of land use and stormwater management on fecal coliform contamination in North Carolina streams. Science of the Total Environment 603-604: 709-727.

Wellen, C., Kamran-Disfani, A.R., Arhonditsis, G.B., 2015. Evaluation of the current state of distributed watershed nutrient water quality modeling. Environmental Science and Technology 49: 3278-3290.

Whitehead, P.G., Leckie, H., Rankinen, K., Butterfield, D., Futter, M.N., Bussi, G., 2016. An INCA model for pathogens in rivers and catchments: Model structure, sensitivity analysis and application to the River Thames catchment, UK. Science of the Total Environment 572: 1601-1610.

Willmott, C.J., Matsuura, K., 2005. Advantages of the mean absolute error (MAE) over the root mean square error (RMSE) in assessing average model performance. Climate Research 30: 79-82.

Windrum, P., Fagiolo, G., Moneta, A., 2007. Empirical validation of agent-based models: Alternatives and perspectives. Journal of Artificial Societies and Social Simulation 10 (2) 8. http://jasss.soc.surrey.ac.uk/10/2/8.html

Figures

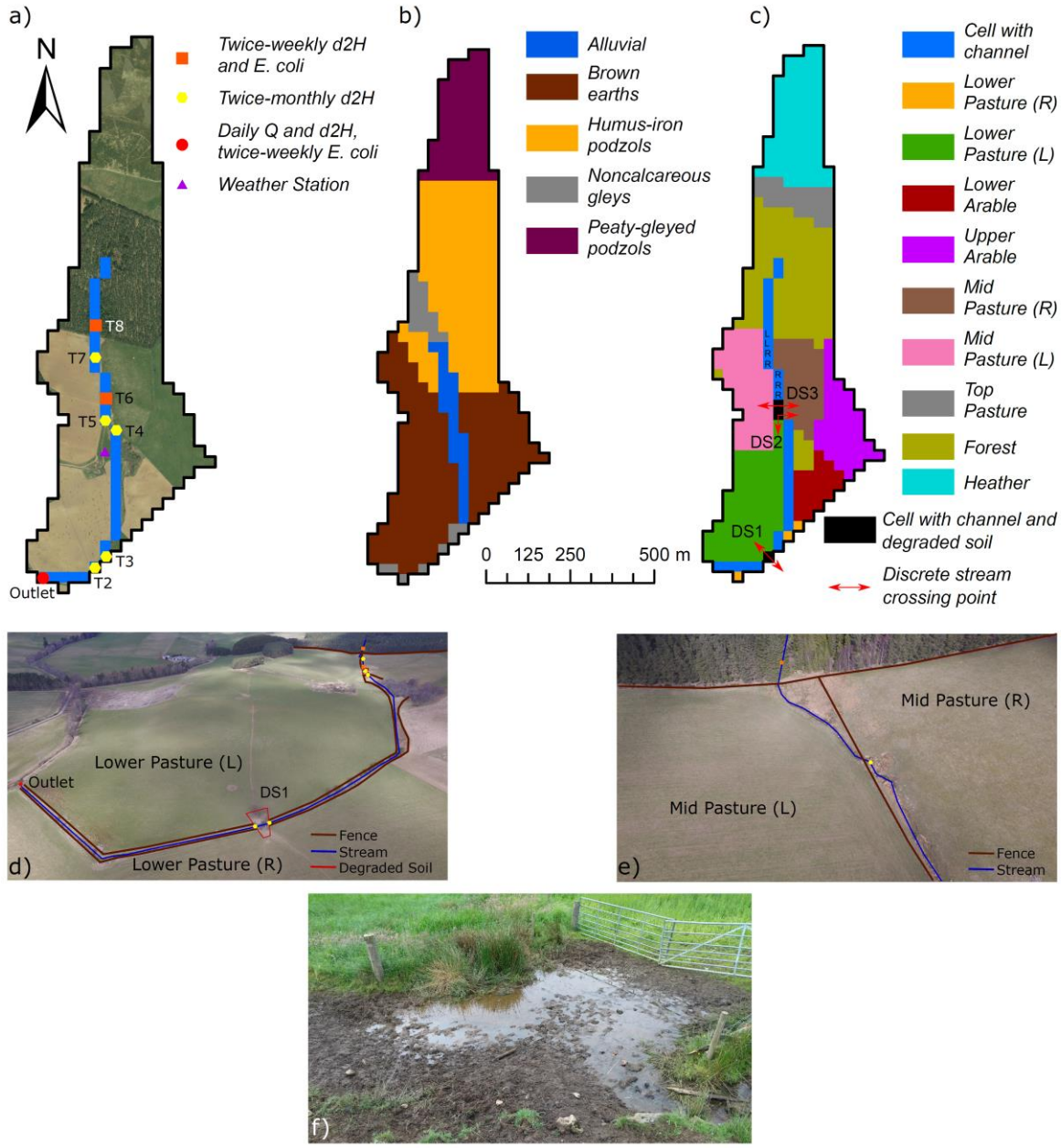

Figure 1: The Tulloch Burn catchment, with maps showing a) An overview of the catchment and monitoring locations; b) Soil types based on Soil Survey of Scotland Staff (2014); c) Designations of land parcels and cells containing a channel (potentially with an area of degraded soil) as provided to MAFIO. In the latter, the appearance of "L" or "R" in cells containing a channel denote the permanent direct accessibility of the stream to livestock in Mid Pastures (L) and (R), respectively, whilst DS1-3 are the designations given to the three areas of degraded soil associated with discrete stream crossing points. The stream in (a) and all data in (b) and (c) are presented on the 30×30 m grid utilised by EcH$_2$O-iso and MAFIO. Also provided are drone-based aerial images of the catchment showing examples of d) Fencing-off of the stream from adjacent fields and areas of soil degradation; e) Sections of the stream

1022 directly accessible to livestock. For context, selected field and degraded soil designations, and
1023 approximate sampling locations are provided in the aerial images using the same symbols as in a). An
1024 example of soil degradation (DS3) in the catchment is shown in (f).

1025

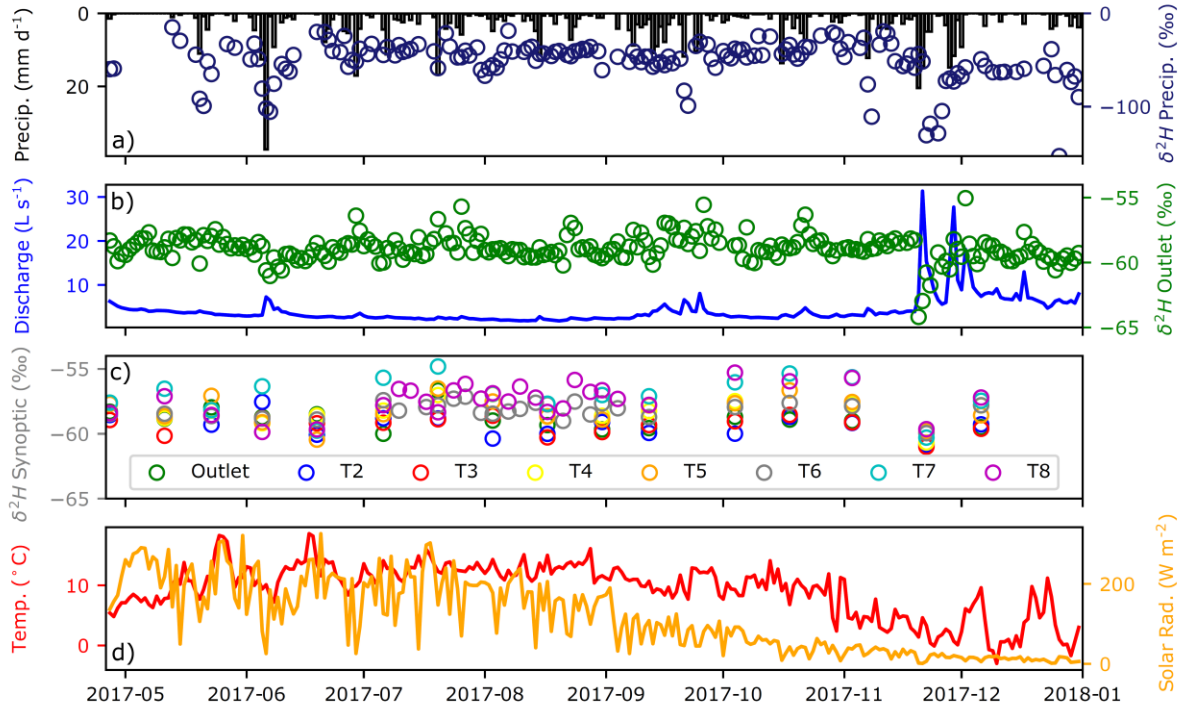

Figure 2: For the full study period, observed timeseries of a) Precipitation and its associated isotopic composition; b) Daily average discharge at the catchment outlet and its associated isotopic composition; c) Isotopic compositions of streamwater at synoptic sampling sites; d) Daily average temperature and solar radiation.

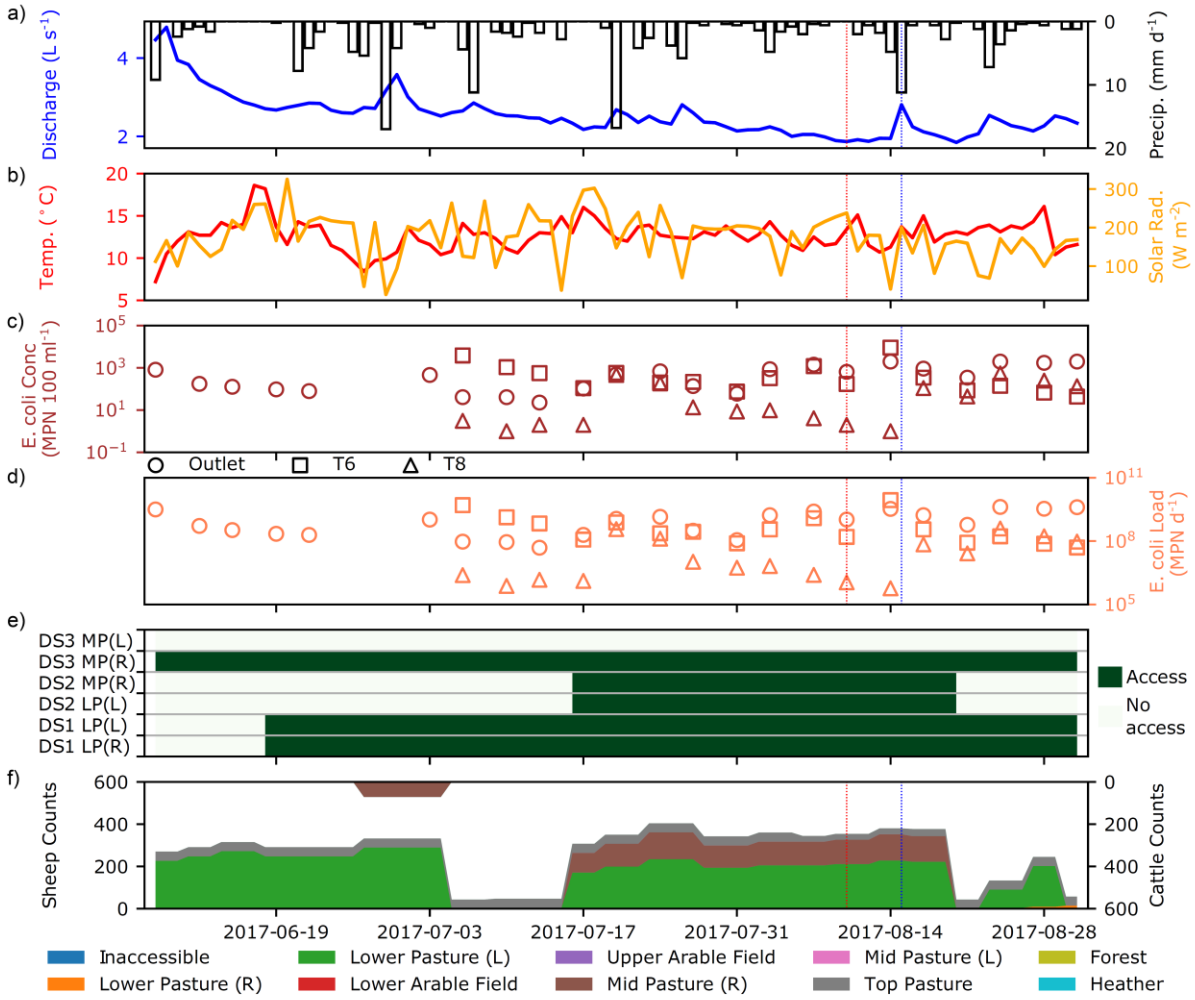

Figure 3: For the microbial observation period, timeseries of observed a) Precipitation and daily average discharge at the catchment outlet; b) Daily average temperature and solar radiation; c) Concentrations of *E. coli* (plotted on a log scale); d) *E. coli* loads (plotted on a log scale); e) Accessibility of the stream to livestock at the discrete crossing points (DS1-3 in Figure 1c); f) Sheep and cattle counts. The red and blue dashed lines denote the example dry and wet days, respectively. In (c) and (d), MPN = most-probable-number. In (e), the abbreviations LP and MP refer to Lower Pasture and Mid Pasture, respectively.

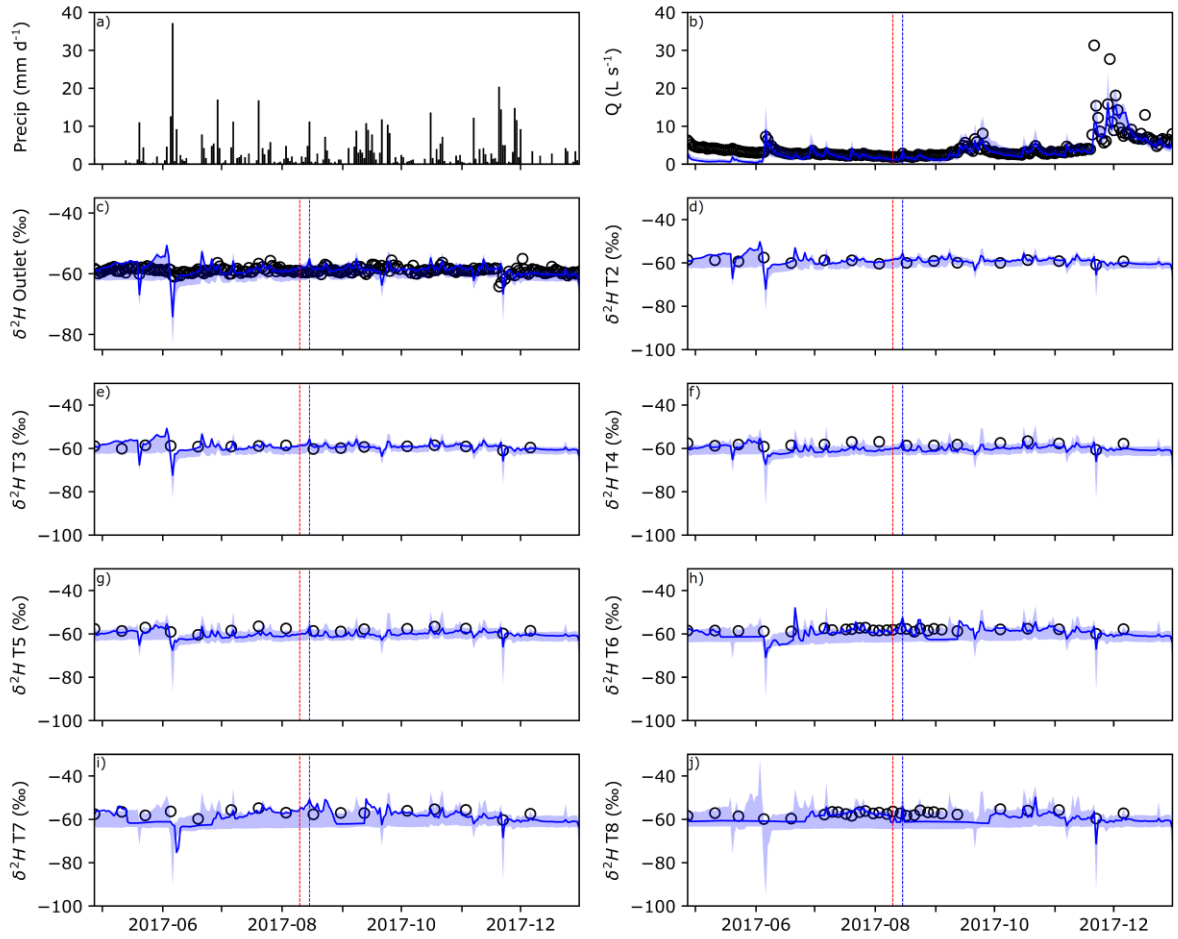

1041

1042 *Figure 4:* Timeseries of a) Precipitation; b) Observed and modelled discharge at the catchment outlet;
1043 c-j) Observed and modelled isotopes at the catchment outlet and synoptic sampling sites. Shaded areas
1044 show the 90% spread of simulations from the behavioural ensemble, whilst the solid blue line shows
1045 the "best" simulation. The red and blue dashed lines denote the example dry and wet days, respectively.
1046 Note the different y-scales between isotope data for the outlet (c) and for the synoptic sampling sites
1047 (d-j), necessary to show the greater spread of the simulations for the latter.

1048

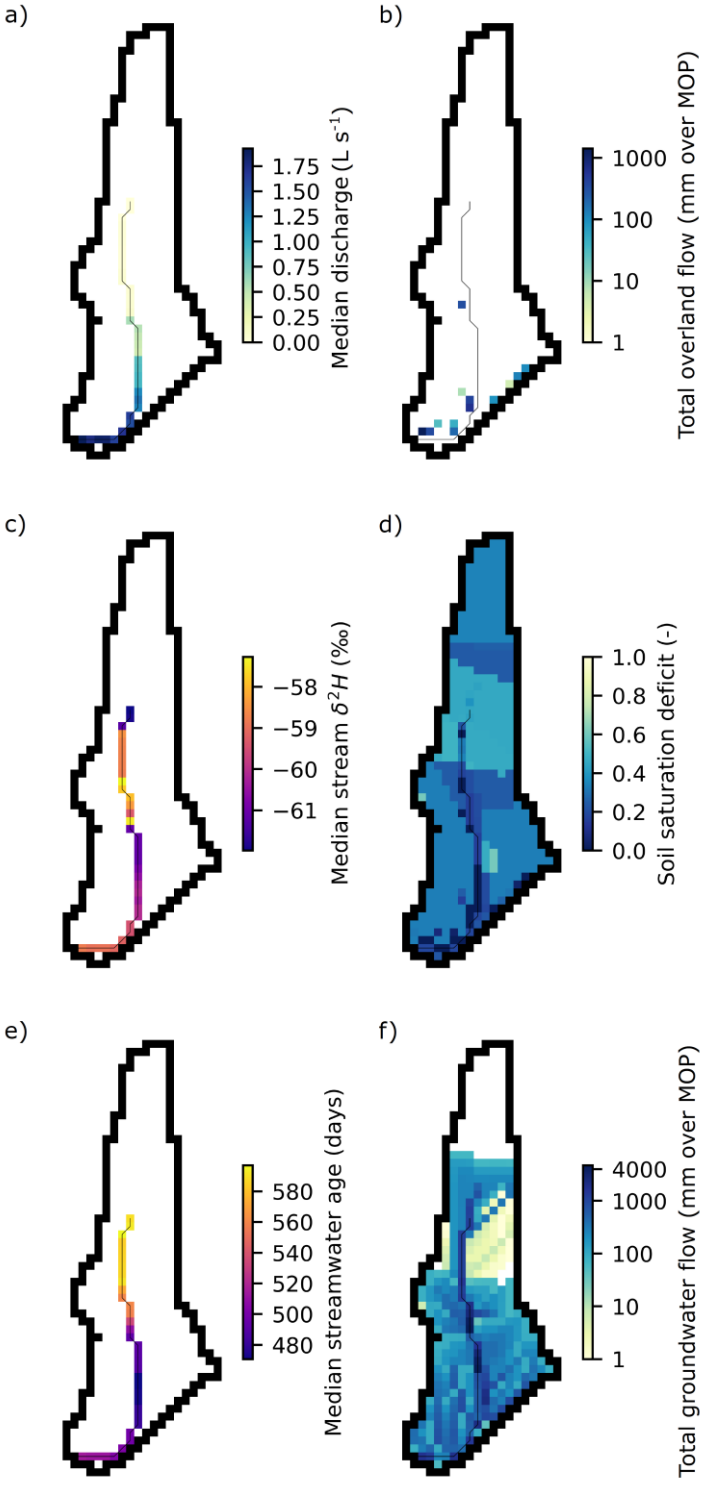

1049

1050 *Figure 5:* Maps showing for the microbial observation period a) Median stream discharge; b) Total
1051 overland flow; c) Median stream δ^2H; d) Median soil saturation deficit; e) Median streamwater age; f)
1052 Total groundwater flow, based on the "best" ensemble run of EcH$_2$O-iso. Overland (b) and groundwater
1053 (f) flows are plotted on log scales for clarity, with areas of white denoting fluxes of 0. MOP = Microbial
1054 observation period.

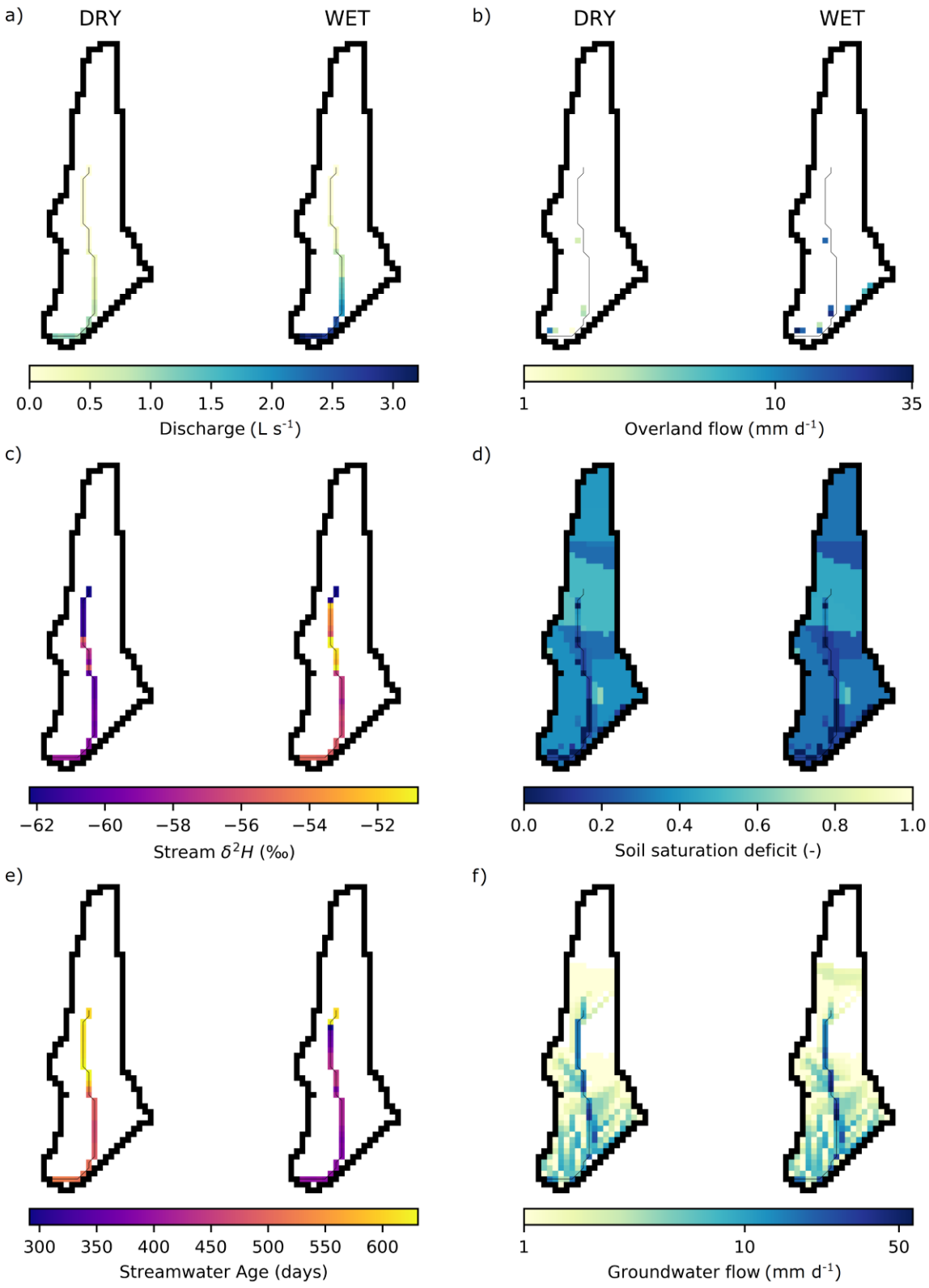

1055

1056 *Figure 6:* For the example dry and wet days, maps showing a) Discharge; b) Overland flow; c)
1057 Streamwater δ^2H; d) Soil saturation deficit; e) Streamwater age; f) Groundwater flow, based on the
1058 "best" ensemble run of EcH$_2$O-iso. Overland (b) and groundwater (f) flows are plotted on log scales for
1059 clarity, with areas of white denoting fluxes of 0.

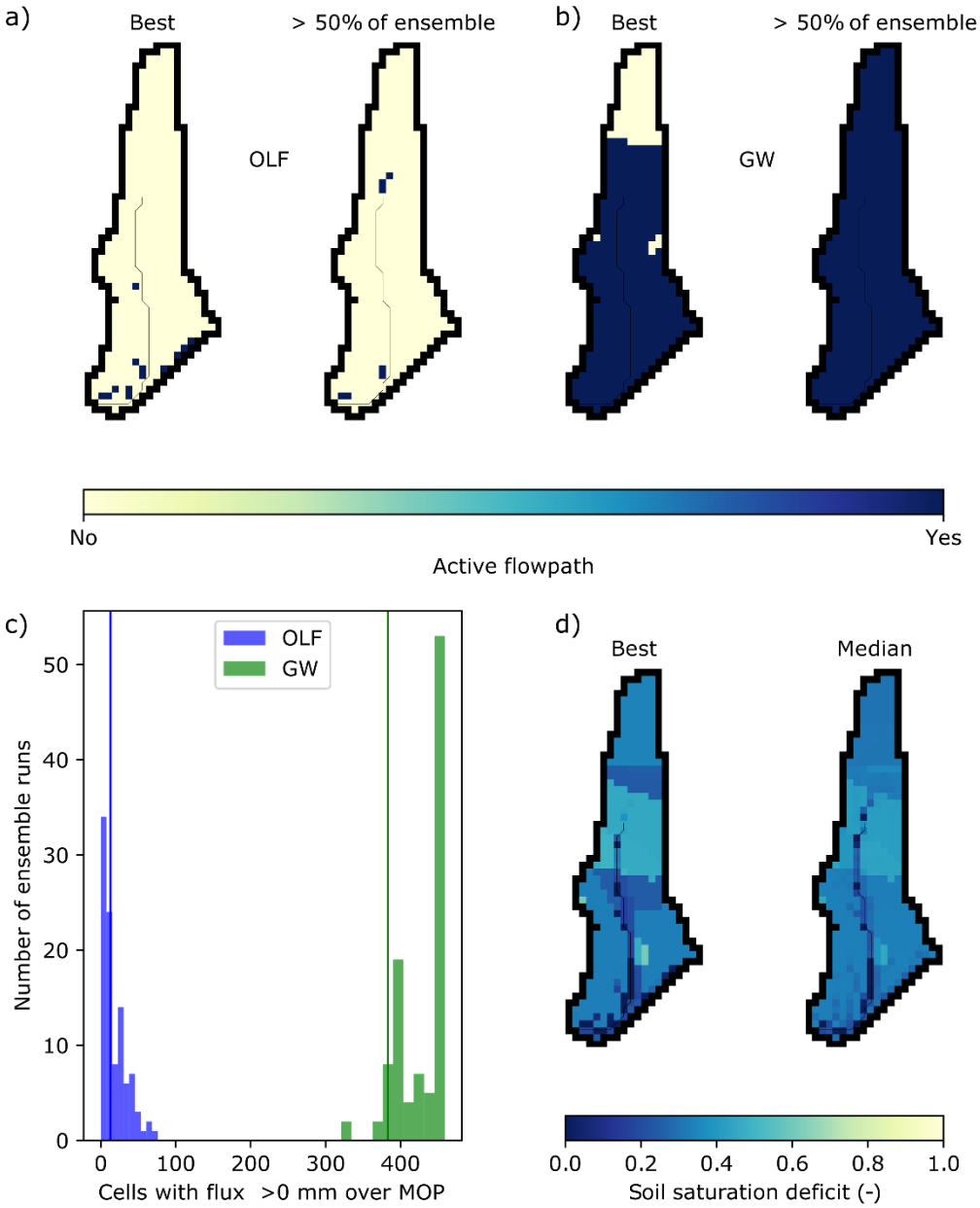

Figure 7: Comparison of spatial simulations made by the "best" run of EcH$_2$O-iso and by an ensemble of 100 behavioural runs: a) Spatial extent of cells with total overland flow (OLF) fluxes greater than 0 mm over the microbial observation period (i.e. "Active flowpath") simulated by the "best" run and >50% of the ensemble; b) As (a) but for groundwater (GW); c) Histogram quantifying the number of ensemble runs in which different numbers of cells were simulated to have total OLF or GW fluxes greater than 0 mm over the microbial observation period (solid lines denote the "best" run); d) Spatial patterns of median soil saturation deficit over the microbial observation period simulated by the "best" run and of the median of the median deficits simulated by the behavioural ensemble. MOP = Microbial observation period.

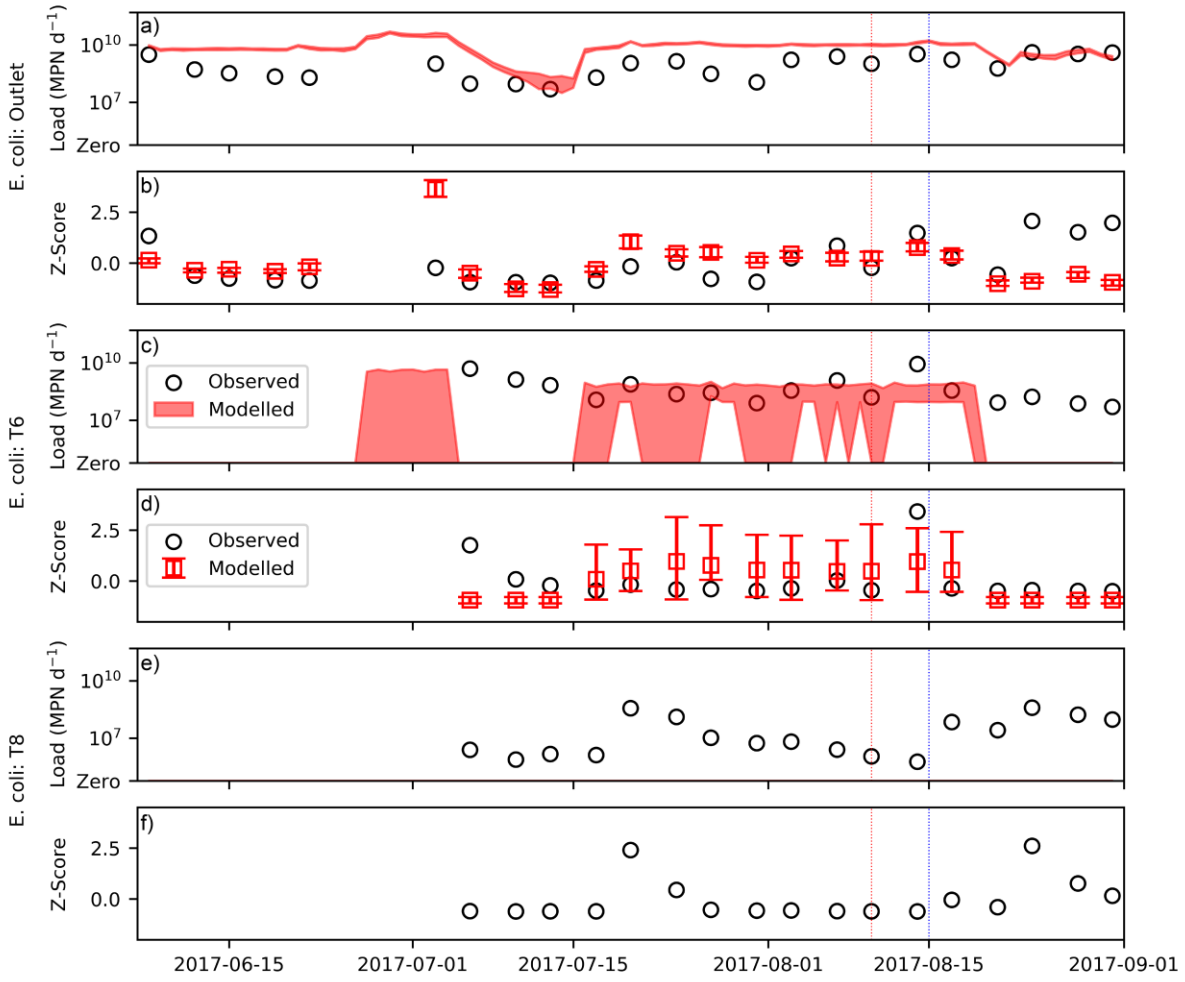

Figure 8: Comparison of observed and simulated *E. coli* loads and Z-scores for a-b) The catchment outlet; c-d) T6; e-f) T8. In the latter, only observed Z-scores are given due to all ensemble runs of MAFIO simulating fluxes of zero FIO-agents for all timesteps. For modelled data, the square marker represents the median Z-score across the 30 ensemble runs of MAFIO, whilst the error bars/shaded areas denote the range of Z-scores/simulated loads. The red and blue dashed lines denote the example dry and wet days, respectively. Loads are plotted on a log scale.

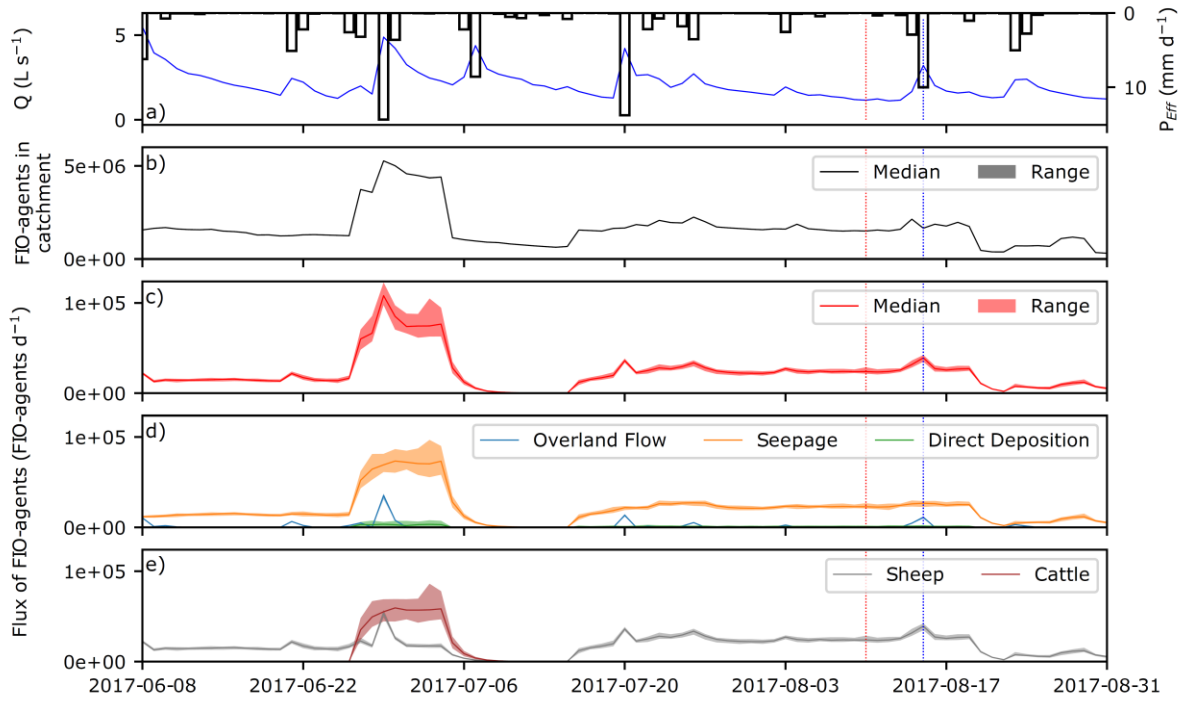

Figure 9: Timeseries of a) Effective precipitation and discharge simulated by the "best" ensemble run of EcH_2O-iso; and b) FIO-agents stored in the catchment at the end of each timestep; c) Flux of FIO-agents exported from the catchment; d) Mechanisms by which exported FIO-agents reached the stream; e) Contributions of exported FIO-agents from sheep and cattle, based on the 30 ensemble runs of MAFIO. The red and blue dashed lines denote the example dry and wet days, respectively. All scales are linear.

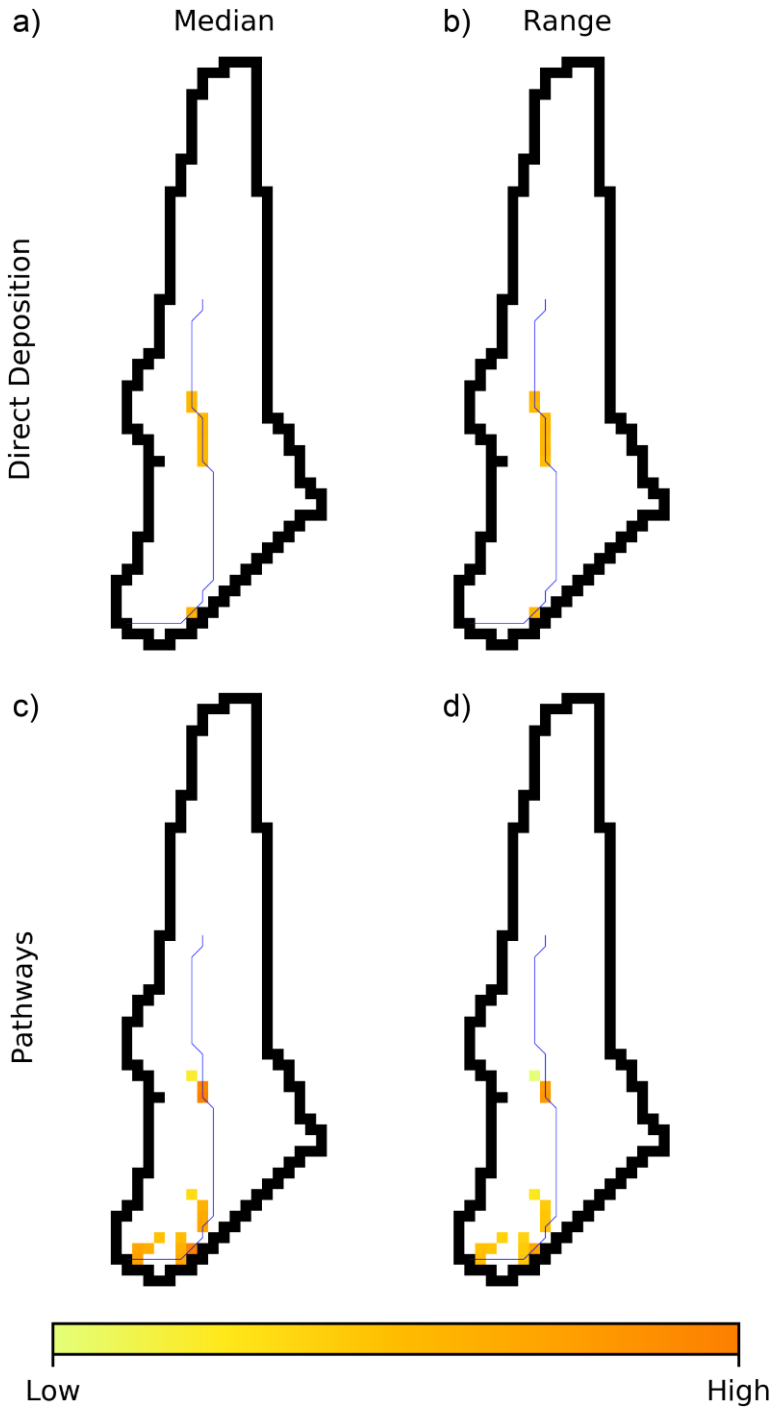

Figure 10: For the whole microbial observation period and based on the 30 ensemble runs of MAFIO, maps showing the median number or range in numbers of exported FIO-agents a-b) Directly deposited in the stream for each cell containing a channel or c-d) That passed through each grid cell in the course of being transported to the stream in overland flow or seepage. The scale reflects the $\log_{10}$-transformed median number/range in numbers and is common to all maps. Areas of white denote medians/ranges of 0.

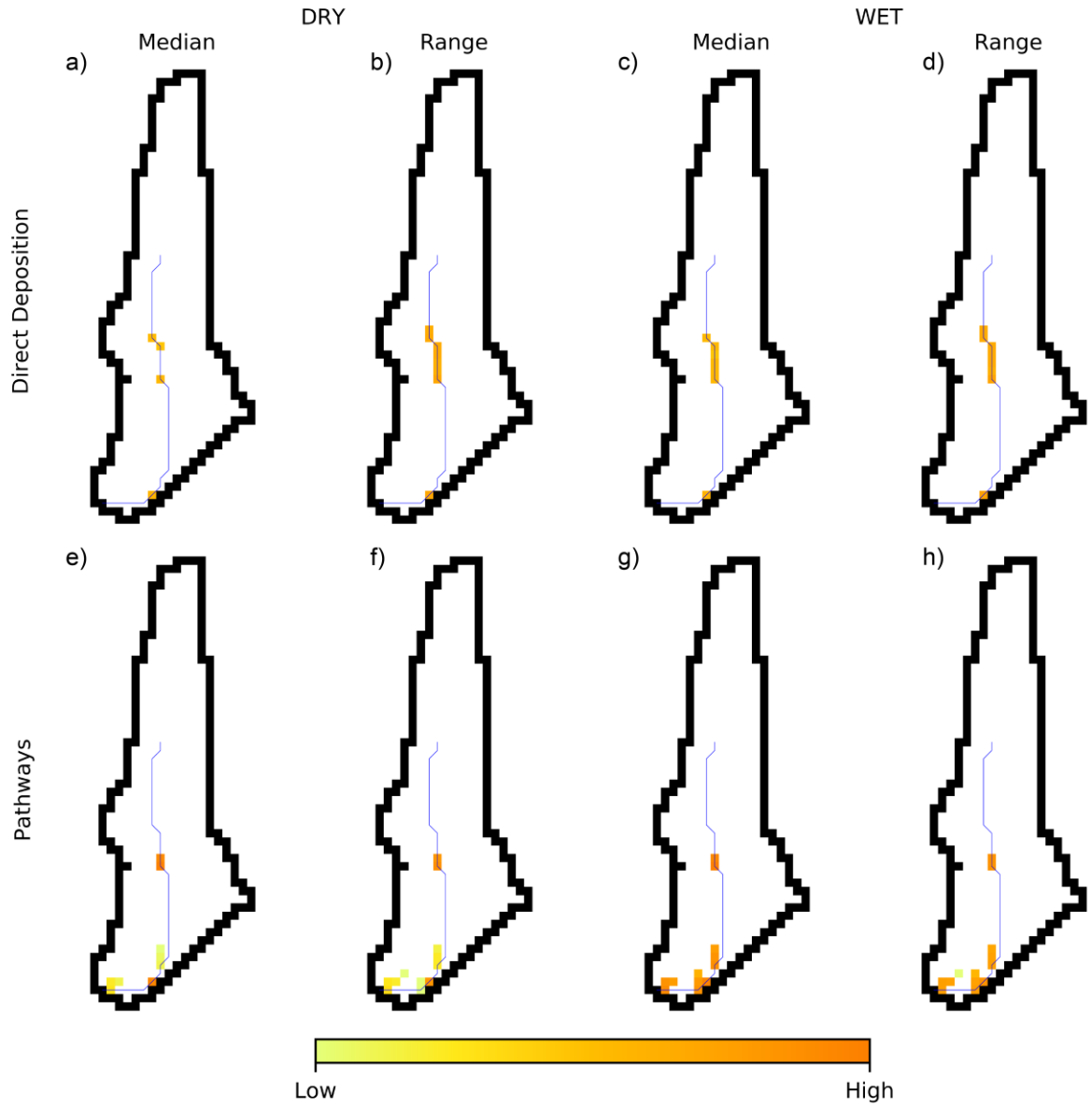

Figure 11: For the exemplar dry day and based on the 30 ensemble runs of MAFIO, maps showing the median number or range in numbers of exported FIO-agents a-b) Directly deposited in the stream for each cell containing a channel or e-f) That passed through each grid cell in the course of being transported to the stream in overland flow or seepage. Equivalent maps for the wet day are shown in (c-d) and (g-h), respectively. The scale reflects the $\log_{10}$-transformed median number/range in numbers and is common to all maps. Areas of white denote medians/ranges of 0.

Tables

Table 1: The number of observations for each calibration target and the weighting for each target in the multi-criteria calibration.

Dataset	Number of observations	Calibration weighting
Discharge: Outlet	249	0.396
Isotopes: Outlet	242	0.385
Isotopes: T2	16	0.025
Isotopes: T3	16	0.025
Isotopes: T4	16	0.025
Isotopes: T5	16	0.025
Isotopes: T6	28	0.045
Isotopes: T7	16	0.025
Isotopes: T8	29	0.046
Total	628	1.0

Table 2: The mean absolute error (MAE) for simulations of discharge and isotope data by the "best" run of EcH_2O-iso (Best MAE), and summary statistics for simulations by the 100 behavioural runs.

Dataset	Best MAE	Mean MAE	Min - Max MAE
Discharge: Outlet	1.37 L s^{-1}	1.56 L s^{-1}	1.24 - 2.04 L s^{-1}
Isotopes: Outlet	1.41‰	1.99‰	1.12 - 3.68‰
Isotopes: T2	1.30‰	2.06‰	1.02 - 3.82‰
Isotopes: T3	1.14‰	2.13‰	0.95 - 3.82‰
Isotopes: T4	2.73‰	3.57‰	0.83 - 6.20‰
Isotopes: T5	2.69‰	3.56‰	1.00 - 6.25‰
Isotopes: T6	2.00‰	3.36‰	0.86 - 6.51‰
Isotopes: T7	3.02‰	4.64‰	1.55 - 8.21‰
Isotopes: T8	2.52‰	4.23‰	1.30 - 8.08‰

Supplementary Material

Appendix A: Parameterisation of EcH$_2$O-iso

The sampling and calibrated ranges of parameters found to be sensitive in EcH$_2$O-iso are given in Table S1, whilst fixed values of insensitive parameters are detailed in Table S2.

Table S1: The sampling and 90%-spread calibrated ranges of soil, vegetation and channel parameters identified as sensitive in the application of EcH$_2$O-iso to Tulloch Burn. Additional information on parameter definitions can be found at: https://ech2o-iso.readthedocs.io/en/latest/Setup.html

Parameter	Sampling range [90% spread of calibrated range]				
Soil	*Brown earths*	*Humus-iron podzol*	*Noncalcareous gley*	*Peaty-gleyed podzol*	*Alluvial*
Total soil depth (m)	1-4 [1.1-3.9]	1-4 [1.1-3.8]	1-4 [1.2-3.8]	1-4 [1.2-3.8]	1-4 [1.3-3.9]
Depth of 1st hydrological layer (m)	0.05-0.25 [0.066-0.25]	0.05-0.25 [0.071-0.24]	0.05-0.25 [0.059-0.24]	0.05-0.25 [0.069-0.24]	0.05-0.25 [0.068-0.24]
Depth of 2nd hydrological layer (m)	0.05-0.5 [0.082-0.49]	0.05-0.5 [0.073-0.48]	0.05-0.5 [0.088-0.49]	0.05-0.5 [0.067-0.45]	0.05-0.5 [0.096-0.45]
Porosity ($m^3\,m^{-3}$)	0.4-0.6 [0.41-0.59]	0.4-0.6 [0.42-0.60]	0.4-0.6 [0.41-0.58]	0.4-0.8 [0.43-0.76]	0.4-0.6 [0.41-0.58]
Porosity exponential decay constant (m^{-1})	1-20 [1.8-18.7]	1-20 [2.1-18.4]	1-20 [1.7-18.0]	1-20 [1.6-19.0]	1-20 [1.9-19.5]
Saturated horizontal hydraulic conductivity (ms^{-1})	1×10^{-5}-0.01 [7.05×10^{-5}-0.0022]	1×10^{-5}-0.01 [9.79×10^{-5}-0.0073]	1×10^{-5}-0.01 [3.72×10^{-4}-0.0087]	1×10^{-5}-0.01 [1.53×10^{-4}-0.0093]	1×10^{-5}-0.01 [2.84×10^{-4}-0.0095]
Hydraulic conductivity exponential decay constant (m^{-1})	1-20 [1.5-18.4]	1-20 [1.6-18.6]	1-20 [2.2-19.3]	1-20 [1.4-19.0]	1-20 [1.6-19.2]
Anisotropy (-)	1×10^{-3}-0.6 [0.035-0.55]	1×10^{-3}-0.6 [0.027-0.58]	1×10^{-3}-0.6 [0.029-0.57]	1×10^{-3}-0.6 [0.043-0.56]	1×10^{-3}-0.6 [0.022-0.57]

Brooks-Corey lambda (-)	3-15 [3.4-13.6]	3-15 [3.4-13.9]	3-15 [3.6-14.6]	3-15 [3.6-14.2]	3-15 [3.5-13.9]
Air-entry pressure head (m)	0.05-0.8 [0.11-0.76]	0.05-0.8 [0.12-0.76]	0.05-0.8 [0.15-0.75]	0.05-0.8 [0.11-0.74]	0.05-0.8 [0.080-0.75]
Tension threshold for mobile water (m)	1-100 [11.3-96.4]	1-100 [12.1-94.8]	1-100 [5.1-94.0]	1-100 [10.4-92.8]	1-100 [6.9-95.3]
Vegetation	*Grasses*	*Conifers*	*Heather*		
Root profile exponential decay constant (m^{-1})	1-20 [2.0-18.9]	1-20 [1.8-18.9]	1-20 [1.9-18.5]		
Maximum stomatal conductance (ms^{-1})	3×10^{-3}-0.05 [0.0039-0.045]	3×10^{-3}-0.05 [0.0068-0.047]	3×10^{-3}-0.05 [0.0048-0.046]		
Soil water potential below which there is complete stomatal closure (-MPa)	2-6 [2.2-5.9]	2-6 [2.3-5.7]	2-6 [2.6-5.8]		
Soil water potential above which there is no soil water limitation to stomatal conductance (-MPa)	0.1-1 [0.18-0.96]	0.1-1 [0.12-0.94]	0.1-1 [0.12-0.93]		
Stomatal sensitivity to light (-)	200-500 [228.9-482.6]	200-500 [223.6-492.0]	200-500 [208.5-488.8]		
Stomatal sensitivity to vapour pressure deficit (-)	1×10^{-3}-3×10^{-3} [1.2×10^{-3}- 2.9×10^{-3}]	1×10^{-3}-3×10^{-3} [1.1×10^{-3}- 2.9×10^{-3}]	1×10^{-3}-3×10^{-3} [1.1×10^{-3}- 2.9×10^{-3}]		
Minimum temperature of comfort (°C)	-5-5 [-4.1-4.4]	-5-5 [-4.5-4.7]	-5-5 [-4.2-4.6]		
Optimal temperature (°C)	6-24 [7.6-23.3]	6-24 [6.9-22.8]	6-24 [6.9-23.2]		
Maximum temperature of comfort (°C)	25-40 [26.0-38.9]	25-40 [26.0-39.9]	25-40 [25.9-38.8]		
Maximum interception storage per unit leaf area index (m)	5×10^{-5}-5×10^{-3} [8.81×10^{-5}- 0.0031]	5×10^{-5}-5×10^{-3} [1.51×10^{-4}- 0.0048]	5×10^{-5}-5×10^{-3} [4.00×10^{-4}- 0.0047]		
Albedo (-)	0.1-0.25 [0.11-0.25]	0.05-0.25 [0.062-0.24]	0.1-0.25 [0.11-0.24]		
Light attenuation coefficient (-)	0.4-0.7 [0.42-0.69]	0.4-0.7 [0.42-0.68]	0.4-0.8 [0.42-0.76]		

Emissivity (-)	0.9-0.99 [0.91-0.99]	0.9-0.99 [0.90-0.99]	0.9-0.99 [0.90-0.98]
Channel			
Resistance to groundwater seepage to channel (-)	5×10^{-3}-0.5 [0.028-0.47]		
Manning's n	1-50 [8.2-47.5]		

1123

1124 *Table S2: Fixed values of uncalibrated parameters in EcH$_2$O-iso*

1125

Parameter	Value					Source
Soil	*Brown earths*	*Humus-iron podzol*	*Non - calcareous gley*	*Peaty-gleyed podzol*	*Alluvial*	
Terrain random roughness (-)	0.05					Maneta and Silverman, 2013
Residual soil moisture ($m^3\ m^{-3}$)	Min{0.05, 0.25 * Hydrological layer porosity}					*Local expertise*
Soil to bedrock leakance (-)	0					*Local expertise*
Soil albedo	0.3					Maneta and Silverman (2013)
Soil emissivity	0.98					Maneta and Silverman (2013)
Heat capacity of dry soil ($J\ m^3\ K^{-1}$)	1.12×10^6	1.19×10^6	1.11×10^6	1.20×10^6	1.10×10^6	*Local expertise*
Thermal conductivity of dry soil ($W\ m^{-1}K^{-1}$)	0.137	0.125	0.138	0.124	0.140	*Local expertise*
Soil depth with negligible heat exchange (m)	2					Maneta and Silverman (2013)
Temperature at bottom thermal layer (°C)	10					Maneta and Silverman (2013)
Snowmelt coefficient ($m\ s^{-1}\ °C^{-1}$)	4.1×10^{-8}					Maneta and Silverman (2013)
Snow to rain temperature threshold (°C)	2					Maneta and Silverman (2013)
Vegetation	*Grasses*	*Conifers*	*Heather*			

Initial LAI ($m^2 m^{-2}$)	2	2.9	1.6	Albrektson (1984); Calder et al. (1984); Moors et al. (1998)
Stem density (m^{-2}) §	-	0.1	200	*Local expertise*
Vegetation age (years) §	-	30	7	*Local expertise*
Basal area (m^2) §	-	0.0195	1.3×10^{-5}	Albrektson (1984); Wallén (1980)
Vegetation height (m)	0.5	10	0.4	*Local expertise*
Root mass (g m^{-2})	1000	800	250	Aerts et al. (1989) ; Oleksyn et al. (1999)
NPP/GPP Ratio (-)	0.35	0.47	0.47	Lozano-Parra et al. (2014)
Canopy quantum efficiency (gC J^{-1})	1.8×10^{-6}	3.0×10^{-6}	1.8×10^{-6}	Landsberg et al. (2005)
Max forest age (years) §	-	500	40	Landsberg et al. (2005)
Leaf carbon allocation coefficient a (-)§	-	2.235	2.235	Lozano-Parra et al. (2014)
Leaf carbon allocation coefficient b (-)§	-	0.006	0.006	Lozano-Parra et al. (2014)
Stem carbon allocation coefficient a (-)§	-	3.3	3.3	Lozano-Parra et al. (2014)
Stem carbon allocation coefficient b (-)§	-	3.0×10^{-7}	3.0×10^{-7}	Lozano-Parra et al. (2014)
Wilting point ($m^3 m^{-3}$)	0.05	0.12	0.06	Maneta and Silverman (2013)
Specific leaf area ($m^2 g^{-1}$)	2.3×10^{-2}	8.0×10^{-3}	9.5×10^{-3}	Landsberg et al. (2005); Poorter and De Jong (1999)

Specific root area (m^2 kg^{-1})	1.1×10^{-2}	6.5×10^{-2}	2.2×10^{-2}	Kuppel et al. (2018)
Crown to stem diameter ratio (-)§	-	0.25	0.25	Landsberg and Waring (1997)
Tree shape coefficient (-)§	-	0.4	0.4	Landsberg and Waring (1997)
Wood density (gC m^{-2}) §	-	2.2×10^{5}	2.2×10^{5}	Landsberg and Waring (1997)
Maximum tree height to stem diameter ratio (-)§	-	15	150	Landsberg and Waring (1997); Wallén (1980)
Minimum tree height to stem diameter ratio (-)§	-	5	5	Landsberg and Waring (1997)
Leaf turnover rate (s^{-1})	3.17×10^{-8}	1.20×10^{-8}	1.00×10^{-8}	Lozano-Parra et al. (2014); Maneta and Silverman (2013)
Max leaf turnover rate under water stress (s^{-1}) §	-	1.8×10^{-8}	1.8×10^{-8}	Landsberg and Waring (1997)
Sensitivity of leaf turnover rate to water stress (-)§	-	0.2	0.2	Landsberg and Waring (1997)
Max leaf turnover rate under temperature stress (s^{-1}) §	-	1.8×10^{-8}	1.8×10^{-8}	Landsberg and Waring (1997)
Sensitivity of leaf turnover rate to temperature (-)§	-	1.8×10^{-8}	1.8×10^{-8}	Landsberg and Waring (1997)
Cold temperature stress threshold (°C) §	-	1	1	Landsberg and Waring (1997)
Root turnover rate (s^{-1})	3.17×10^{-8}	2.7×10^{-8}	1.0×10^{-8}	Landsberg and Waring (1997)
Canopy-scale water use efficiency (gC m^{-1})	800	680	3335	Gordon et al. (1999); Hobbie and Colpaert, (2004)

Empirical tree water use coefficient (-)[§]	-	0.6	0.6	Landsberg and Waring (1997)
Empirical tree water use exponent (-)[§]	-	7	7	Landsberg and Waring (1997)
Dry grass decomposition rate (s^{-1}) [¢]	8.5×10^{-7}	-	-	Lozano-Parra et al. (2014)
Temperature threshold triggering dry grass decay (°C) [¢]	18	-	-	Lozano-Parra et al. (2014)

[§] Ligneous species only; [¢] Herbaceous species only

1126

1127

Appendix B: Sub-grid characterisation of channel cells in MAFIO

To enable sub-grid heterogeneity in MAFIO to be represented, it is necessary to specify several characteristics for cells containing an area of degraded soil / the channel. Figure S1 shows the Seepage and Channel IDs associated with such cells and their corresponding upslope contributing cells. The latter are used in deriving attributes of the spatial grid for the former. Channel widths, land parcels and livestock access associated with each cell are given in Table S3.

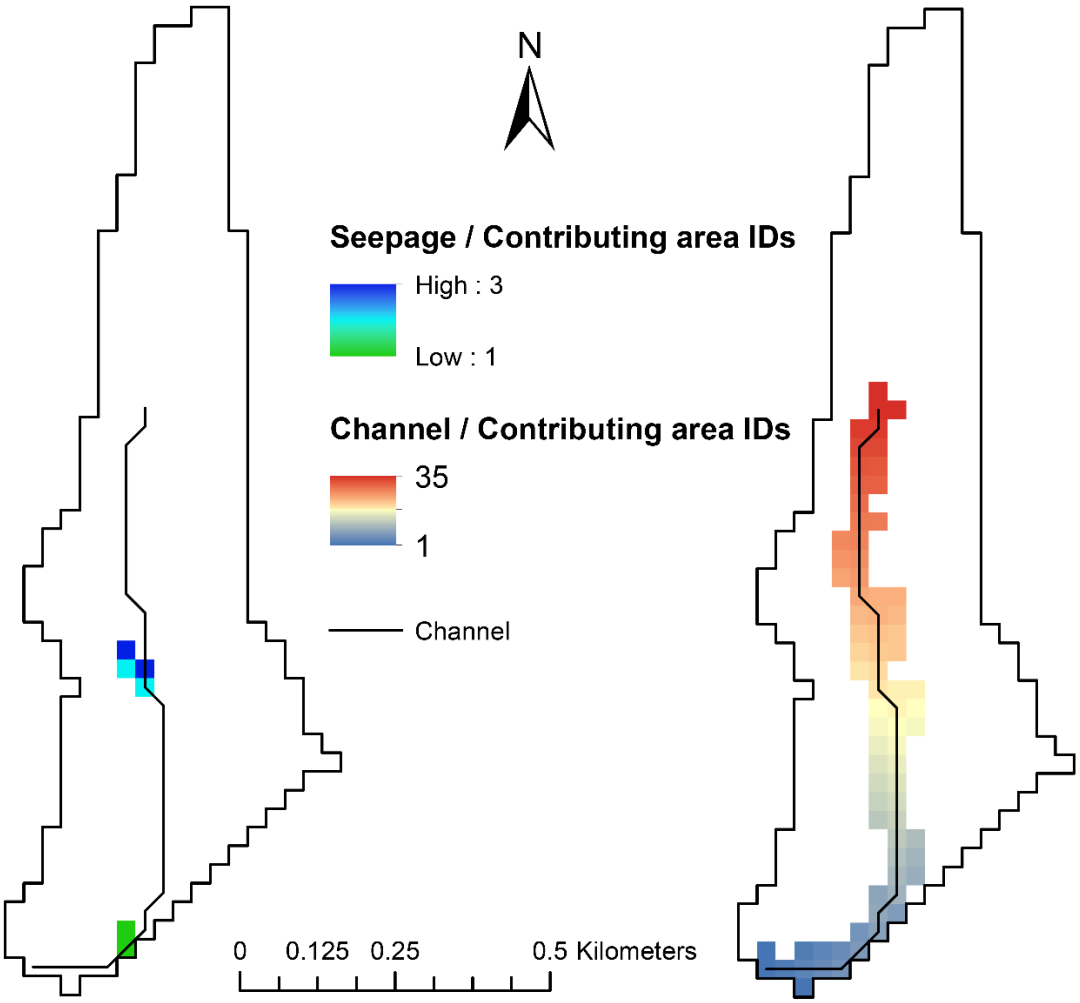

Figure S1: Maps showing a) The seepage IDs of cells with areas of degraded soil and their associated immediate upslope contributing areas; b) The channel IDs of cells containing a channel and their associated immediate upslope contributing areas. Cells containing the area of degraded soil / channel are those intersected by the "Channel" line.

Table S3: The properties of cells containing areas of degraded soil / the channel necessary for the representation of sub-grid heterogeneity.

Channel ID	Seepage ID	Channel Width (m)	Land parcel(s)	Livestock Access
1	-	0.37	Lower Pasture (L) and (R)	No
2	-	0.37	Lower Pasture (L) and (R)	No
3	-	0.40	Lower Pasture (L) and (R)	No
4	-	0.45	Lower Pasture (L) and (R)	No
5	-	0.48	Lower Pasture (L) and (R)	No
6	1	0.51	Lower Pasture (L) and (R)	Gate*
7	-	0.55	Lower Pasture (L) and (R)	No
8	-	0.57	Lower Pasture (L) and (R)	No
9	-	0.62	Lower Pasture (L) and (R)	No
10	-	0.64	Lower Pasture (L) and Lower Arable	No
11	-	0.61	Lower Pasture (L) and Lower Arable	No
12	-	0.59	Lower Pasture (L) and Lower Arable	No
13	-	0.57	Lower Pasture (L) and Lower Arable	No
14	-	0.54	Lower Pasture (L) and Lower Arable	No
15	-	0.53	Lower Pasture (L) and Forest	No
16	-	0.52	Lower Pasture (L) and Forest	No
17	-	0.49	Lower Pasture (L) and Forest	No
18	-	0.43	Forest	No
19	-	0.37	Forest	No
20	2	0.32	Lower Pasture (L) and Mid Pasture (R)	Gate*

21	3	0.40	Mid Pastures (L) and (R)	Yes for (R); Gate* for (L)
22	-	0.48	Mid Pastures (L) and (R)	Yes for (R)
23	-	0.52	Mid Pastures (L) and (R)	Yes for (R)
24	-	0.50	Mid Pastures (L) and (R)	Yes for (R)
25	-	0.46	Mid Pastures (L) and (R)	Yes for (R)
26	-	0.44	Mid Pastures (L) and (R)	Yes for (R)
27	-	0.41	Mid Pasture (L)	Yes
28	-	0.35	Mid Pasture (L)	Yes
29	-	0.30	Forest	Yes
30	-	0.26	Forest	Yes
31	-	0.21	Forest	Yes
32	-	0.17	Forest	Yes
33	-	0.12	Forest	Yes
34	-	0.06	Forest	Yes
35	-	0.01	Forest	Yes

* Variable livestock access depending on gate opening

1141

1142

1143

References

Aerts, R., Berendse, F., Klerk, N. M. and Bakker, C., 1989. Root production and root turnover in two dominant species of wet heathlands, Oecologia 81(3): 374–378.

Albrektson, A. (1984). Sapwood basal area and needle mass of Scots pine (Pinus sylvestris L.) trees in central Sweden. Forestry 57(1): 35–43.

Calder, I.R., Hall, R.L., Harding, R.J., Wright, I.R., 1984. The use of a wet-surface weighing lysimeter system in rainfall interception studies of heather (Calluna vulgaris). Journal of Climate and Applied Meteorology 23(3): 461–473.

Gordon, C., Woodin, S.J., Mullins, C.E., Alexander, I.J., 1999. Effects of environmental change, including drought, on water use by competing Calluna vulgaris (heather) and Pteridium aquilinum (bracken). Functional Ecology 13(s1): 96–106.

Hobbie, E.A., Colpaert, J.V., 2004. Nitrogen availability and mycorrhizal colonization influence water use efficiency and carbon isotope patterns in Pinus sylvestris. New Phytologist 164(3): 515–525.

Kuppel, S., Tetzlaff, D., Maneta, M.P., Soulsby, C., 2018. What can we learn from multi-criteria calibration of a process-based ecohydrological model? Environmental Modelling and Software 101: 301-316.

Landsberg, J., Mäkelä, A., Sievänen, R., Kukkola, M., 2005. Analysis of biomass accumulation and stem size distributions over long periods in managed stands of Pinus sylvestris in Finland using the 3-PG model. Tree Physiology 25(7): 781–792.

Landsberg, J.J., Waring, R.H., 1997. A generalised model of forest productivity using simplified concepts of radiation-use efficiency, carbon balance and partitioning. Forest Ecology and Management 95(3): 209–228.

Lozano-Parra, J., Maneta, M..P., Schnabel, S., 2014. Climate and topographic controls on simulated pasture production in a semiarid Mediterranean watershed with scattered tree cover. Hydrology and Earth Systems Science 18: 1439.

Maneta, M.P., Silverman, N.L., 2013. A spatially distributed model to simulate water, energy, and vegetation dynamics using information from regional climate models. Earth Interactions 17(11): 1–44.

Moors, E., Stricker, J. van der Abeele, G. (1998) Evapotranspiration of cut over bog covered by Molinia Caerulea. Wagenigen.

Oleksyn, J., Reich, P.B., Chalupka, W., Tjoelker, M.G., 1999. Differential Above- and Below-ground Biomass Accumulation of European Pinus sylvestris Populations in a 12-year-old Provenance Experiment. Scandinavian Journal of Forest Research 14(1): 7-17.

Poorter, H., De Jong, R.O.B., 1999. A comparison of specific leaf area, chemical composition and leaf construction costs of field plants from 15 habitats differing in productivity. New Phytologist 143(1): 163–176.

1178 Wallén, B., 1980. Structure and Dynamics of Calluna Vulgaris on Sand Dunes in South Sweden. Oikos 35(1): 20.